DEVELOPMENT OF THE BIAXIAL STRESS TEST FOR SHEET MATERIAL

By

PETER H. ALBERTIN, M.Eng.(Welding)

A Thesis

Submitted to the School of Graduate Studies

in Partial Fulfilment of the Requirements

for the Degree

Master of Engineering

(Production)

McMaster University

(March) 1972

MASTER OF ENGINEERING (1972) McMASTER UNIVERSITY
(Production) Hamilton, Ontario

TITLE: DEVELOPMENT OF THE BIAXIAL STRESS TEST FOR SHEET MATERIAL

AUTHOR: Peter H. Albertin, M.Eng. (Welding)
Gdansk University

SUPERVISOR: Dr. J. L. Duncan

NUMBER OF PAGES: ix, 91

SCOPE AND CONTENTS:

The basic information about sheet metal testing and material formability are given and present theories in this area are briefly reviewed.

The hydrostatic bulge test is an established method of testing sheet metal under equal biaxial tension, and previous developments are reviewed.

The primary object of this project has been the design, development, and manufacture of new biaxial test equipment. A fast method of calculating a representative stress - strain curve using this equipment is described.

Advantages resulting from the utilization of this testing unit and some laboratory experiments using this equipment are described.

ACKNOWLEDGMENTS

The author sincerely appreciates the guidance, support and, above all, encouragement throughout this work given by Dr. J. L. Duncan of McMaster University.

The author also wishes to acknowledge the financial support for completion of this thesis given by McMaster University and the National Research Council.

Acknowledgment is given to the technical staff of the machine shop at McMaster University and particularly to superintendent Mr. R. W. Young.

TABLE OF CONTENTS

LIST OF FIGURES

LIST OF FIGURES (cont'd)

LIST OF SYMBOLS

ε	- logarithmic or material strain
ε_1, ε_2, ε_3	- principal strains
ε_t	- thickness strain
ε_o	- strain indicating initial state of the material
ε^*	- instability thickness strain
ε_{Tave}	- average tensile strain
$d\varepsilon_1$; $d\varepsilon_2$	- strain increment in x, y direction
ε_z	- normal strain
σ	- membrane stress at the pole
σ_1, σ_2, σ_3	- principal stresses
σ_z	- normal stress
$\bar{\sigma}$	- representative stress
σ_o	- basic strength of the material independent of its initial state
σ_{Tave}	- average tensile stress
R_θ	- normal anisotropy parameter
ΔR	- planar anisotropy
$\bar{R}$	- average normal anisotropy parameter
R	- normal plastic anisotropy
p	- pressure
ρ	- radius at curvature
D_o	- initial diameter
D_1	- current diameter

w_o - initial width

w - current width

t_o - initial thickness

t - current thickness

n - index of rate of hardning with strain

P - tensile force

A - area

1. INTRODUCTION

Sheet metal forming is a large and economically important activity, and also a finely developed art. Every day millions of components are pressed from sheet metal under conditions which successfully, but only very narrowly, avoid the ever present dangers of either tearing or buckling of the sheet.

The principal purpose in testing sheet metal is to be able to select the cheapest grade of sheet which will just form into the desired shape and in a highly developed technique such as pressing or deep drawing, very small differences in material properties can make the difference between success or scrap metal.

The usual criterion for failure in sheet metal working is whether the part forms without tearing and without developing a visible local strain concentration.

There are a large number of mechanical tests for sheet material but in most of them, the parameter measured depends on a large number of basic material properties and test variables. The quantitative information from such a test indicates often the interaction of many different properties rather than absolute measure of any one property.

A number of the fundamental properties of sheet metal such as the initial yield stress, the strain hardening

characteristic and the degree of anisotropy can be derived from the simple tension test. There are however certain disadvantages to this test; the test specimen must be carefully prepared to avoid the effects of strain hardening of the edges of the test piece and an accurate measurement technique must be used to quantify anisotropy. The main disadvantage however is that, for many materials, the maximum strain is limited by the onset of necking. It is, of course, important that the range of strain in a mechanical test should extend over the range of effective strain in the forming process being investigated.

The maximum effective strain in some stretching processes may reach about 0.8 and in deep-drawing it may be as high as 1.0* equivalent to 272% elongation. These are, of course, much greater than the maximum uniform strains in the tension test.

Some of the above difficulties are not present in the hydrostatic bulge test and this test is an extremely useful one for sheet metal. In the bulge test, a circular specimen is clamped rigidly at the periphery and subjected to uniform hydrostatic pressure on one side of the specimen. The deformation of a thin circular diaphragm has been studied extensively during the last twenty years. Such a stressed diaphragm is stretch-

*Strains given as logarithmic or natural strains $\varepsilon = \ln\frac{l}{l_o}$ where l = current and l_o initial gauge length.

formed into a symmetrical spherical dome and in the central or polar region of this dome, a state of approximately uniform biaxial stress and strain is created where large values of strain may be expected to occur before rupture. From measurement of radius of curvature, surface extension and bulging pressure, a stress - strain curve can be derived.

The maximum uniform strain is greater than in the simple tension test and in general the range of the bulge test covers the range in any real sheet metal forming operation.

2. LITERATURE SURVEY

2.1 General

In forming sheet metal, the physical boundary of the material is constantly changing and critical conditions can occur at any point in the process. Therefore, better understanding of the formability of sheet metal is essential for the production of high quality stampings.

It is understood that techniques such as the use of incipient slip line fields in solid mechanics and steady state fields and velocity discontinuity methods in extrusion, rolling and metal-cutting are not generally applicable in sheet metal forming processes.

Most of the metal sheets used for forming processes are anisotropic. The parameters defining the state of anisotropy in sheet metal can be determined from the strain ratios of tensile specimens aligned parallel perpendicular and at some intermediate orientation, usually 45°, to the direction of rolling. This parameter is defined as,

$$R_\theta = \frac{\ln(w/wo)}{\ln(t/to)} \qquad (2.1.1)$$

Equality of the strain ratios at any angle θ, does not guarantee isotropy. Complete isotropy requires all strain ratios to be equal to unity. If $R_\theta = R_o = R_{90} \leq 1$, then only normal anisotropy is present.

Planar anisotropy is defined in terms of strain ratios recorded from the different directions as

$$\Delta R = \frac{1}{2}(R_0 - 2R_{45} + R_{90}) \quad (2.1.2)$$

while the average normal anisotropy is defined as

$$\bar{R} = \frac{1}{4}(R_0 + 2R_{45} + R_{90}) \quad (2.1.3)$$

The strain hardening characteristic of a material is generallyindicated by the exponent n in the expression

$$\bar{\sigma} = \sigma_o(\varepsilon_o + \bar{\varepsilon})^n \quad (2.1.4)$$

or for fully annealed materials,

$$\bar{\sigma} = \sigma_o\bar{\varepsilon}^n \quad (2.1.5)$$

where σ_o is some measure of the basic strength of the material independent of its initial state; ε_o provides an indication of the initial state of the material, and n is a measure of the rate of hardening with strain. The value of σ_o is independent of the amount of strain that a material can withstand, but does determine the stress necessary to attain any given value of strain.

Bramley and Mellor (2) tested four different steel sheets with anisotropic properties and compared the strain hardening characteristic obtained from the tensile test specimen in the different rolling direction of the sheet. On the basis of the equivalence of plastic work during deformation, the relationships between the strain hardening characteristics when measured trans-

versely and parallel to the direction of rolling in the plane of the sheet are given by

$$\sigma_{90} = \left[\frac{1 + 1/R_o}{1 + 1/R_{90}} \right]^{\frac{1}{2}} \sigma_o \qquad (2.1.6)$$

$$\varepsilon_{90} = \left[\frac{1 + 1/R_{90}}{1 + 1/R_o} \right]^{\frac{1}{2}} \varepsilon_o$$

Extending this principle of the equivalence of plastic work to a sheet of material subjected to balanced biaxial tension along the anisotropic axes in the plane of the sheet, the strain hardening characteristics perpendicular to the sheet can be predicted theoretically as shown by Venter (8) from either of the relations

$$\sigma_z = \left[\frac{1 + R_o}{1 + R_o/R_{90}} \right]^{\frac{1}{2}} \sigma_o \quad , \quad \varepsilon_z = \left[\frac{1 + R_o/R_{90}}{1 + R_o} \right]^{\frac{1}{2}} \varepsilon_o \qquad (2.1.7)$$

and, or

$$\sigma_z = \left[\frac{1 + R_{90}}{1 + R_{90}/R_o} \right]^{\frac{1}{2}} \sigma_{90} \quad , \quad \varepsilon_z = \left[\frac{1 + R_{90}/R_o}{1 + R_o} \right]^{\frac{1}{2}} \varepsilon_{90}$$

Venter in (8) says that the predicted values show poor correlation with the experimental strain hardening characteristics perpendicular to the sheet, and consequently raise the question whether the work hardening associated with an anisotropic material is solely dependent

upon the plastic work per unit volume (3).

An improved correlation still based on the equivalence of plastic work, can be obtained if an average $\bar{R}$ value is used as given by equation (2.1.3) or calculated from the area under the experimental curves relating R to the degree of orientation from the direction of rolling. The relationships are then given by

$$\sigma_z = \left[\frac{1 + \bar{R}}{2}\right]^{\frac{1}{2}} \sigma_{ave} \qquad \varepsilon_z = \left[\frac{2}{1 + \bar{R}}\right]^{\frac{1}{2}} \varepsilon_{ave} \quad (2.1.8)$$

A different way of calculating the average $\bar{R}$ value was suggested by Professor Duncan in (4) based on stress measurements at different points on the expanding yield locus:

$$\bar{R} = 2\left[\frac{\sigma_z}{\frac{1}{4}(\sigma_o + 2\sigma_{45} + \sigma_{90}}\right]^{\frac{2}{n+1}} - 1 \qquad (2.1.9)$$

where σ_o, σ_{45} and σ_{90} are the uniaxial stresses obtained from tensile specimen orientated at 0^o, 45^o, and 90^o to the direction of rolling, and σ_z is the stress perpendicular to the plane of the sheet obtained from a circular bulge test and all stresses correspond to the same defined level of strain. Equation (2.1.9) cannot be obtained by a rigorous analysis as a number of assumptions are employed, and in a material which does not exhibit planar isotropy, equality of uniaxial strain does not correspond with equality of total plastic deformation.

2.2 Plastic Instability

In industrial applications each forming process can be considered as a unique combination of drawing and stretch-forming operations, and as such it becomes increasingly difficult to analyse since the relative influence of both mechanisms is basically unknown.

Numerous authors (5 - 8) have successfully investigated the individual mechanisms associated with the stretch forming and deep drawing of sheet metal by constructing, testing and analysing experimental models which are predominantly draw or stretch type processes but there are no generally accepted theories which completely describe the way in which sheet metal ruptures under biaxial tension. Those theories which associate failure with the attainment of a maximum in traction forces in the sheet or in overall applied loading are not entirely satisfactory.

Goodwin (9) has measured the strains normal and parallel to the point of fracture, for sheet which has failed under biaxial tension, and produced a so called "forming limit diagram". A typical diagram is shown in Fig. 1 for different ratios of biaxial stress and establishes an envelope around the strains which can be reached without fracture. Somewhat earlier Keeler and

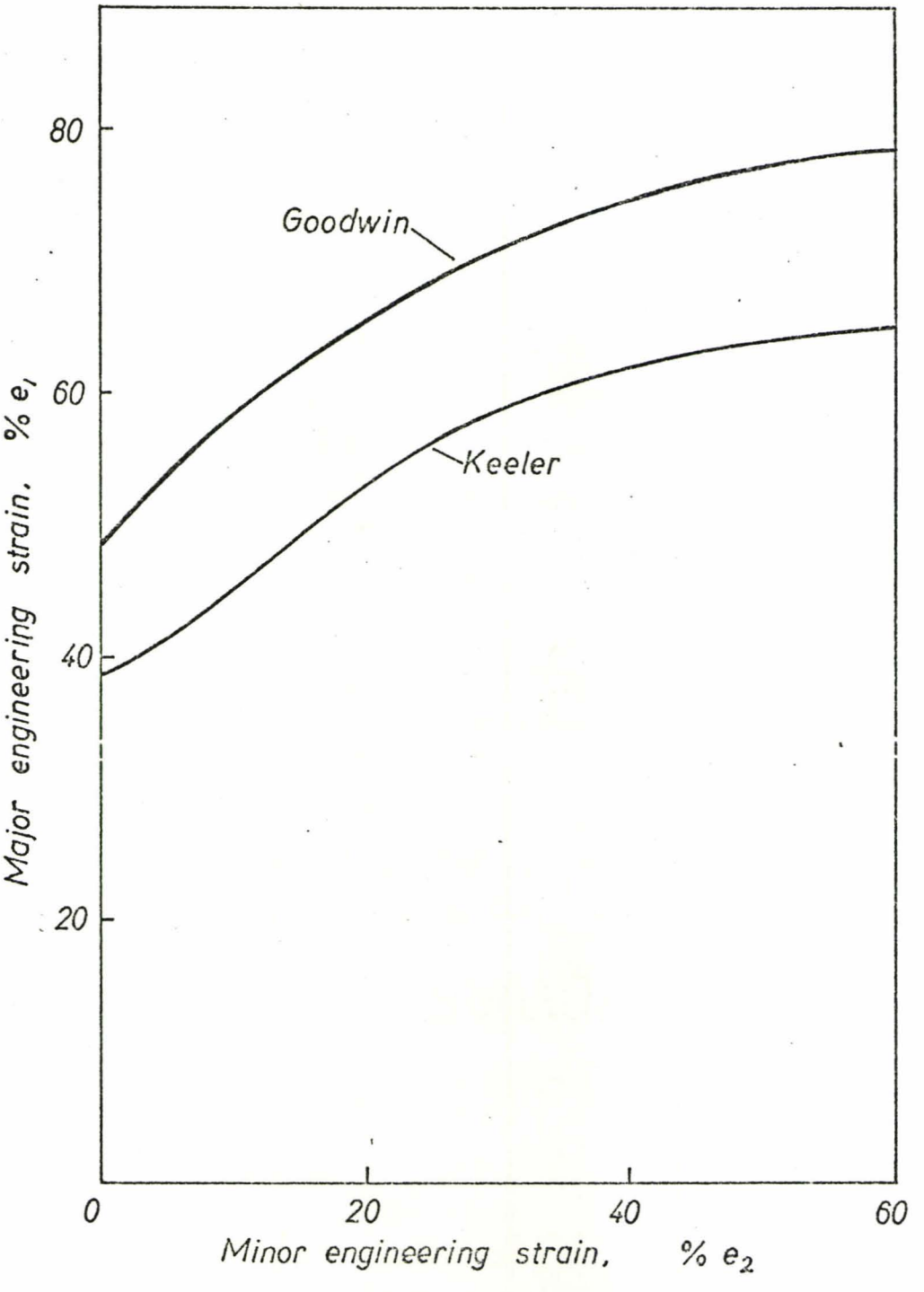

Figure 1.

Keeler - Goodwin formability curve.
After Venter(8).

Backofen had plotted a similar diagram, but rather than measure the strains around the point of fracture he chose to measure them at a sufficient distance away to avoid localized strain gradients. A comparison of the Keeler and Goodwin curves (Fig. 1) suggests that failure is preceded by a localized strain concentration similar to that occuring in a local neck in simple tension. Fig. 1 shows that there is a significant difference between the maximum strains of the fracture site - the Goodwin curve - and the limit strains - the Keeler curve - and this suggests that there is some very localized deformation process which precedes actual fracture in biaxial stretching processes. It is unlikely that the maximum useful strain in a process - the limit strain - can be predicted theoretically either from consideration of fracture alone or simply from a stability of diffuse necking analysis.

A hypothesis which appears to describe the localized deformation process leading to fracture in biaxial tension has been developed by Marciniak (10). The theory predicts the effect of changes in the measurable material properties on the limit strains and provides an extremely useful concept of failure in sheet metal. The theory is extensive and includes all of the major material parameters known to affect formability. The

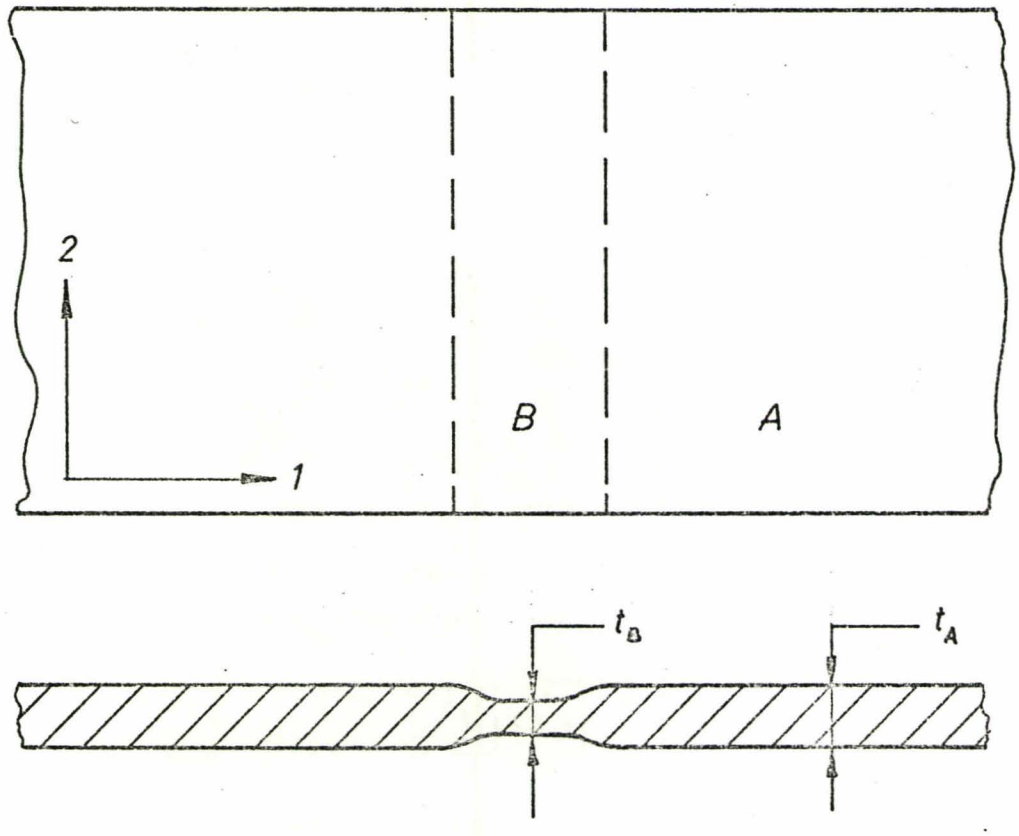

Figure 2.
Element of a sheet deforming in biaxial tension containing a grooved region B.
After Sowerby and Duncan (11)

hypothesis depends on the assumption that the sheet is initially inhomogeneous, and that as the sheet is stretched a suitable disposed inhomogeneity will develop into a groove which is assumed to run perpendicular to the direction of the greatest principal stress σ_1 (Fig. 2). It was assumed by Marciniak that the incremental strain in this direction, $d\varepsilon_1$, develops at a different rate inside and outside the groove; but the incremental strain along the groove, $d\varepsilon_2$, is assumed equal in both regions. As the deformation proceeds the current strain ratio in the groove, ie. $\left(\frac{d\varepsilon_1}{d\varepsilon_2}\right)_B$ will be greater than that in the general vicinity ie. $\left(\frac{d\varepsilon_1}{d\varepsilon_2}\right)_A$ and thus the groove will deepen. The ratio $\left(\frac{d\varepsilon_1}{d\varepsilon_2}\right)_A$ is assumed constant throughout the process and can be computed from the appropriate flow rule if the stress path $\left(\frac{\sigma_1}{\sigma_2}\right)_A$ is specified. A necessary condition to be satisfied throughout the process is that of equilibrium thus,

$$(\sigma_1 \; t_A)_A = (\sigma_1 \; t_B)_B \qquad (2.2.1)$$

where t_A and t_B are the material thickness outside and inside the groove respectively.

The deformation process, as pointed out by Sowerby and Duncan (11), can be described most conveniently by plotting the loading paths in regions A and B with respect to the appropriate yield locus for the plane stress case Fig. 3. (The shape of the yield surface depends upon the

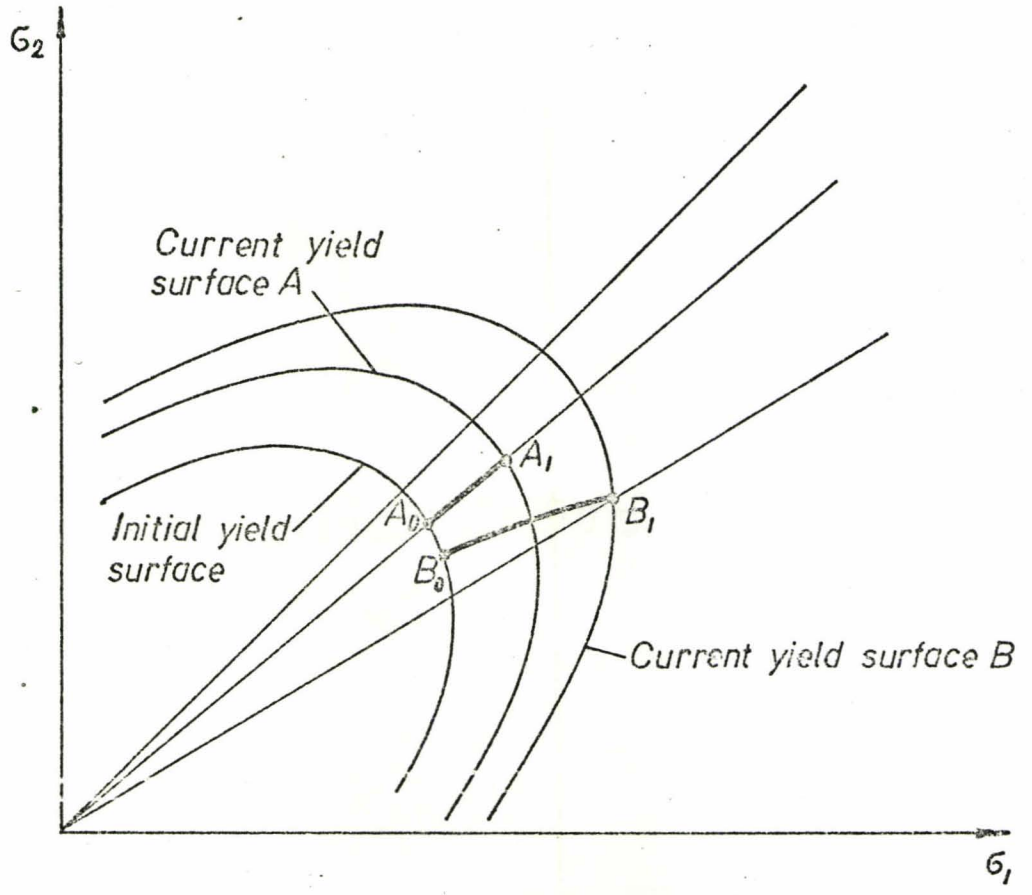

Figure 3.

Principal stresses in each region showing the loading paths from initial yield, A_0, B_0 to failure A_1, B_1.
After Sowerby and Duncan (11).

choice of the yield criterion and whether the material is considered anisotropic. Fig. 3 has been drawn using the von Mises criterion). As shown in Fig. 3 the loading path outside the groove is assumed linear, while that inside the groove is determined by satisfying the equilibrium equation 2.2.1 and the appropriate yield criterion. Straining inside and outside the groove is occuring simultaneously, but the material within the groove is straining at a faster rate. Failure is assumed to occur either when the strains reach some limit of ductility for the material within the groove, i.e. the phenomenon of decohesion takes place, or the strain ratio within the groove $\left(\frac{d\varepsilon_1}{d\varepsilon_2}\right)_B$, approaches infinity. In other words for this latter case the plane strain condition is reached within the groove, which is shown as the position B_1 in Fig. 3.

Three different cases are identified by Sowerby and Duncan (11) to cover the deformation process leading to fracture when the plane strain state is eventually reached within the groove. The one cited above is when straining occurs simultaneously inside and outside the groove.

Alternatively, material in the groove is assumed to yield before that in the immediate vicinity. However, because $d\varepsilon_2$ is specified as being the same in

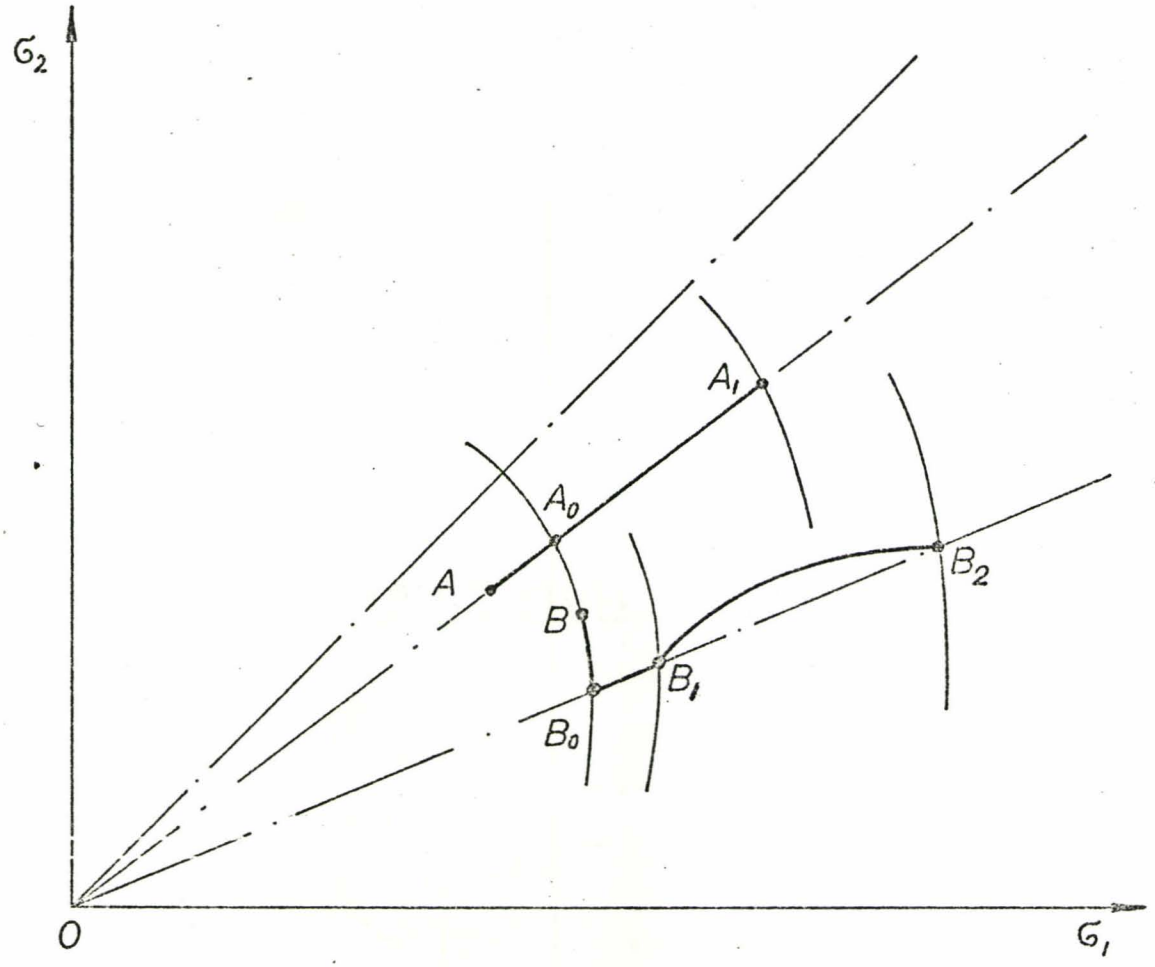

Figure 4.

Principal stress space showing the loading paths for Case 2. After Sowerby and Duncan (11).

both regions, plastic straining can only occur in the groove under conditions of plane strain. This situation does not exist up to fracture but because equation (2.2.1) has to be satisfied, along with the yield criterion, it is necessary in certain cases that material outside of the groove also reaches yield. The stress state inside and outside of the groove at this instance is given by points A_o and B_1 respectively in Fig. 4. As plastic deformation continues (23) says that the stress state in the groove moves away from the plane strain case and then finally back again when fracture finally occurs. The schematic loading path is shown by B_o B_1 B_2 in Fig.4, while the loading path for material outside the groove is along OA_o continued.

The third case discussed by Sowerby and Duncan (11 & 28) is when straining takes place solely in the groove, under conditions of plane strain, up to fracture. The limit strain is the instability strain which is computed in this instance by conventional instability techniques.

2.3 Effect of the strain - hardening index n

The forming limit diagram calculated for an isotropic material R = 1, for different values of n is shown in Fig. 5. Stress strain curve given by Sowerby and Duncan in (11) was obtained from equation

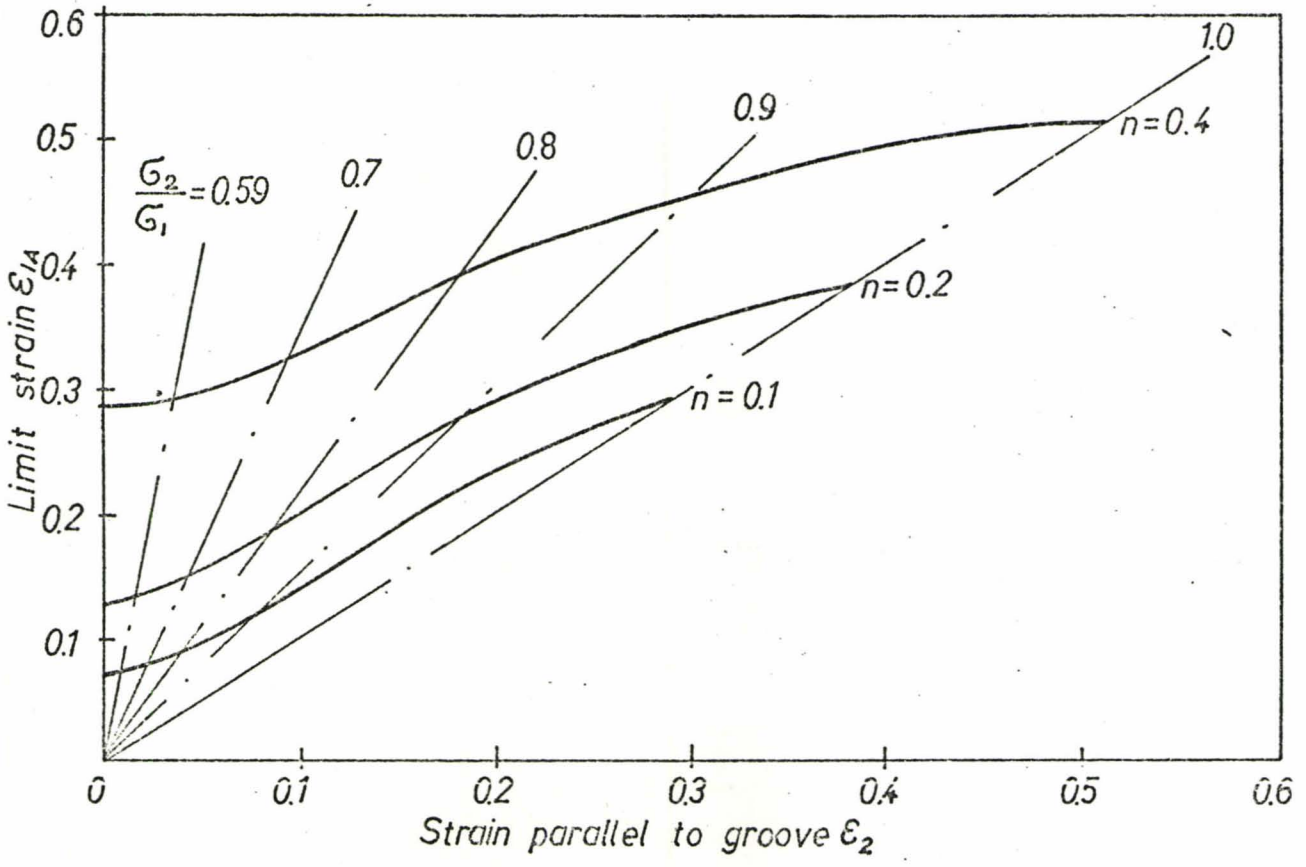

Figure 5.

Theoretical forming limit diagrams for three isotropic materials ($R = 1$, $\varepsilon_0 = 0.0014$, $(t_B/t_A)_0 = 0.98$) showing the influence of the strain-hardening index, n.
After Sowerby and Duncan (11).

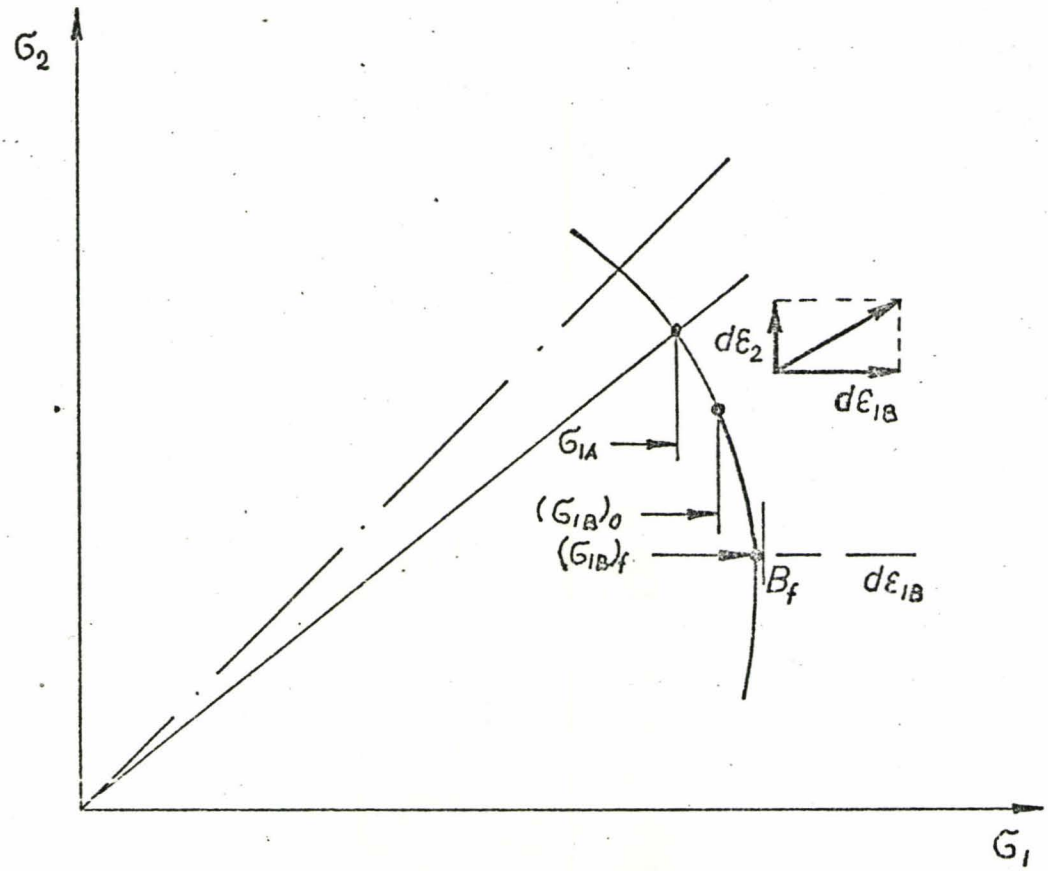

Figure 6.

Principal stresses space for a non-strain-hardening material. After Sowerby and Duncan (11).

$$\bar{\sigma} = \sigma_o(0.0014 + \bar{\varepsilon})^n \qquad (2.3.1)$$

initial inhomogeneity of $t_B/t_A = 0.98$ was taken and value of the initial work hardening: $\varepsilon_o = 0.0014$ was used the same as used by Marciniak. Computation was performed for four stress ratios in the range $\sigma_2/\sigma_1 = .07$ to $\sigma_2/\sigma_1 = 1$ following case 1 described in the previous paragraph, one ratio $\sigma_2/\sigma_1 = 0.592$ following case 2 and one point of the plain strain axis.

It can be noticed that for all cases, the limit strains increases with increasing n. The limit strain for a given n increases as the process moves from plane strain towards equal biaxial tension. Proportionally, the increase in limit strain is greatest for materials having a low strain-hardening index. Practically, this fact is demonstrated by half-hard aluminium, which cannot be stretched to any great extent in uniaxial or plane strain tension but it can be stretched to high values of strain in a circular bulge test. The forming limit diagram for half-hard aluminium is, in fact, similar in shape to the curve for n = 0.1 in Fig. 5. Sowerby and Duncan in (11) suggest that even for n = 0 appreciable straining could be obtained in biaxial tension before failure. This may be appreciated from the yield locus in Fig. 6. If n = 0, the locus does not expand and the stress in the uniform region remains constant and equal to σ_{1A} as shown.

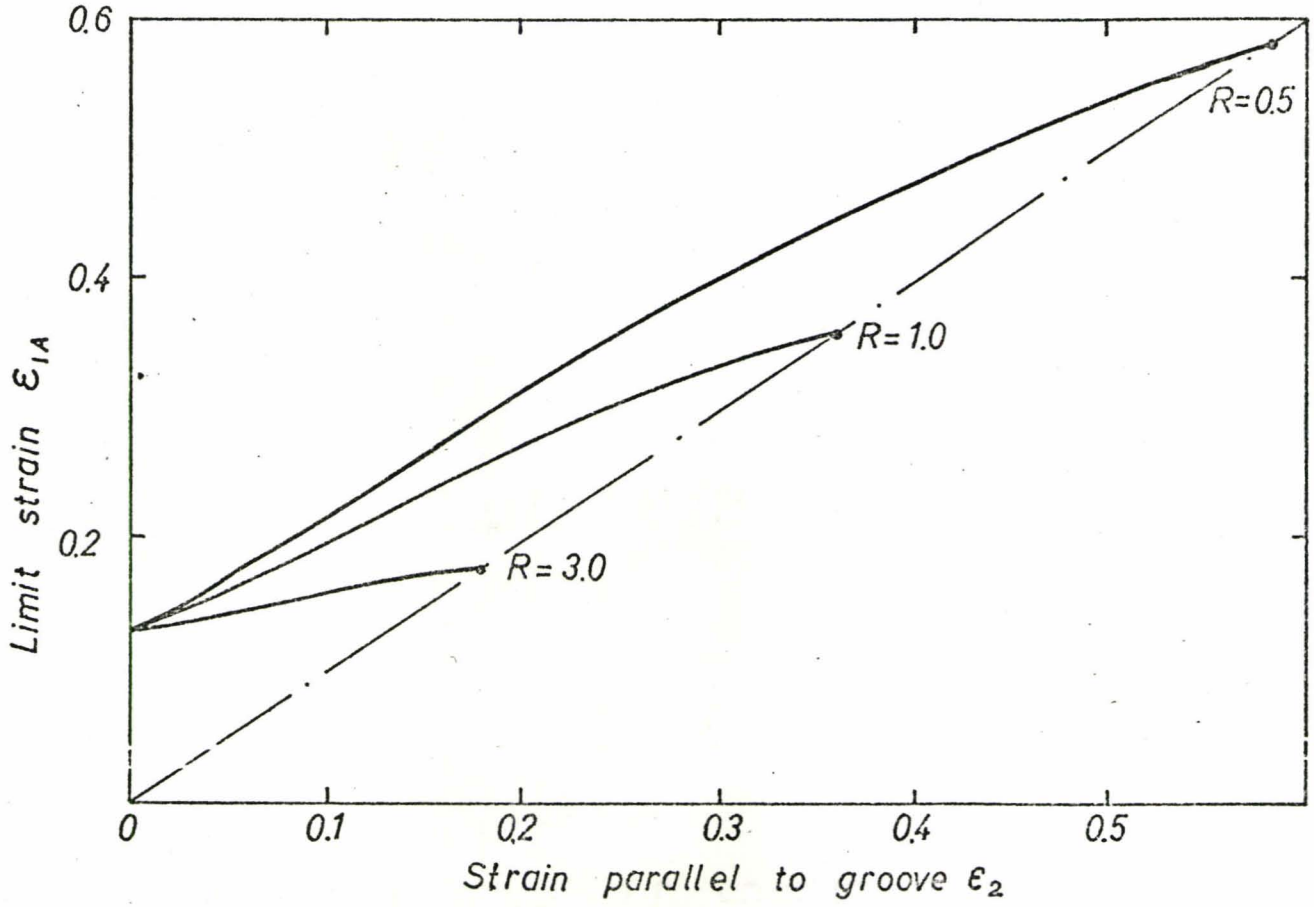

Figure 7.

Theoretical forming limit diagrams for three materials ($\varepsilon_0 = 0.0014$, $n = 0.2$, $(t_3/t_A)_0 = 0.98$) showing the influence of normal plastic anisotropy.
After Sowerby and Duncan (11).

Initially at yield

$$\frac{\sigma_{1A}}{(\sigma_{1B})_o} = \left(\frac{t_B}{t_A}\right)_o \qquad (2.3.2)$$

and as the groove deforms then there is some transverse strain increment $d\varepsilon_2$ as shown in the diagram; the point B will move around the locus to the plane strain point B_f before the transverse strain increment $d\varepsilon_2$ becomes zero. Consequently $\varepsilon_2 = \int d\varepsilon_2$ will have some finite value and as the strain ratio $\varepsilon_{1A}/\varepsilon_2$ is at all times constant, there must be some finite straining in the uniform region prior to failure.

The diagram shown in Fig.5 considered materials having the same anisotropy value R = 1, but the situation is different when R varies.

2.4 Effect of the anisotropy value R

The forming limit diagrams calculated for materials having constant n and ε_o but different R are discussed by Sowerby and Duncan in (11 & 28) as shown in Fig. 7. For stretching processes approximating to equal biaxial tension an increase in the R value decreases the limit strain. Fig.7 suggests that stretch-forming requires material having high n and low R. The reason for this can be deduced from the yield locus. If R increases, the elliptical yield locus is "stretched out" along the equal biaxial tension axis $(\sigma_1/\sigma_2)_A = 1$ as

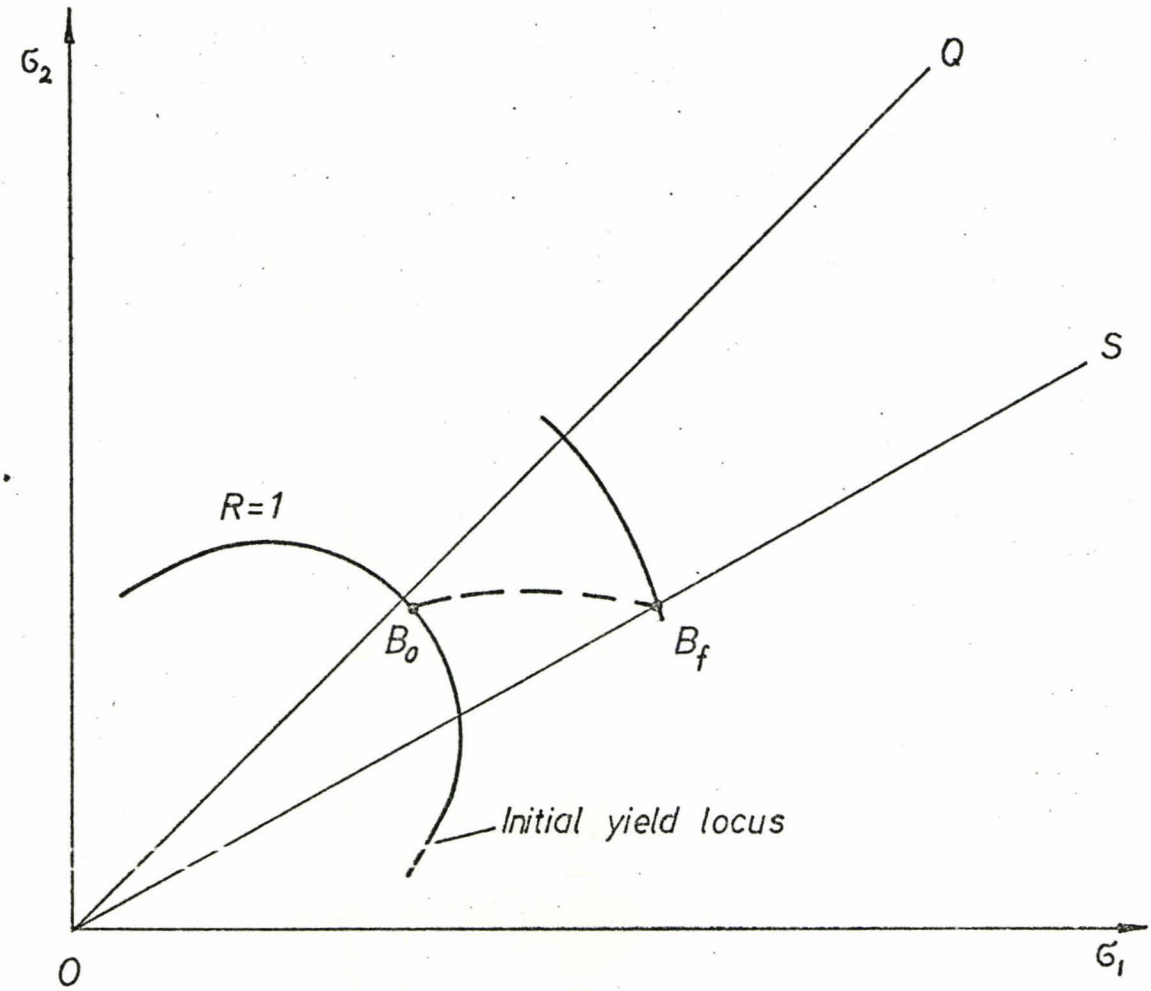

Figure 8.

Yield locus and loading path for isotropic sheet. After Sowerby and Duncan (11).

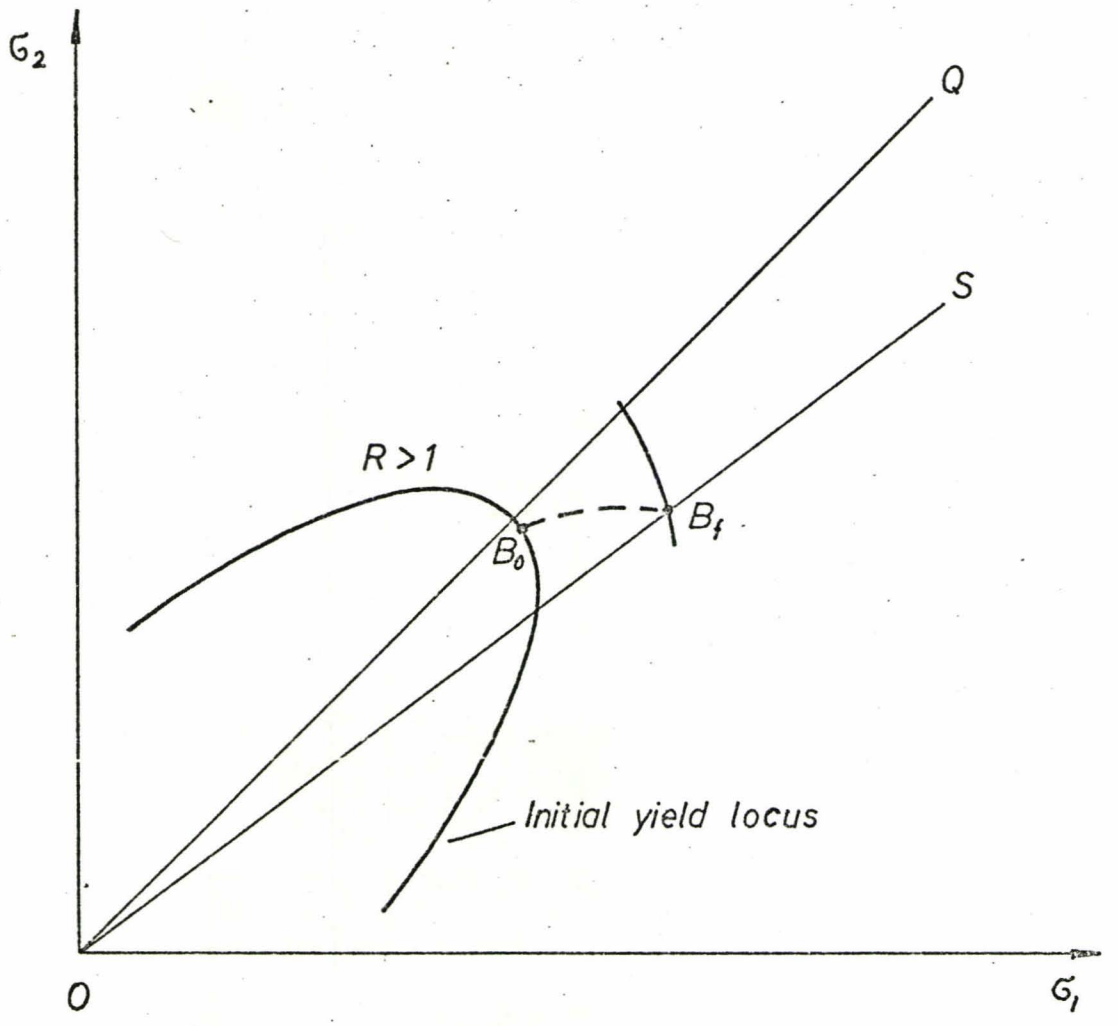

Figure 9.

Yield locus and loading path for high R-value sheet. After Sowerby and Duncan (11).

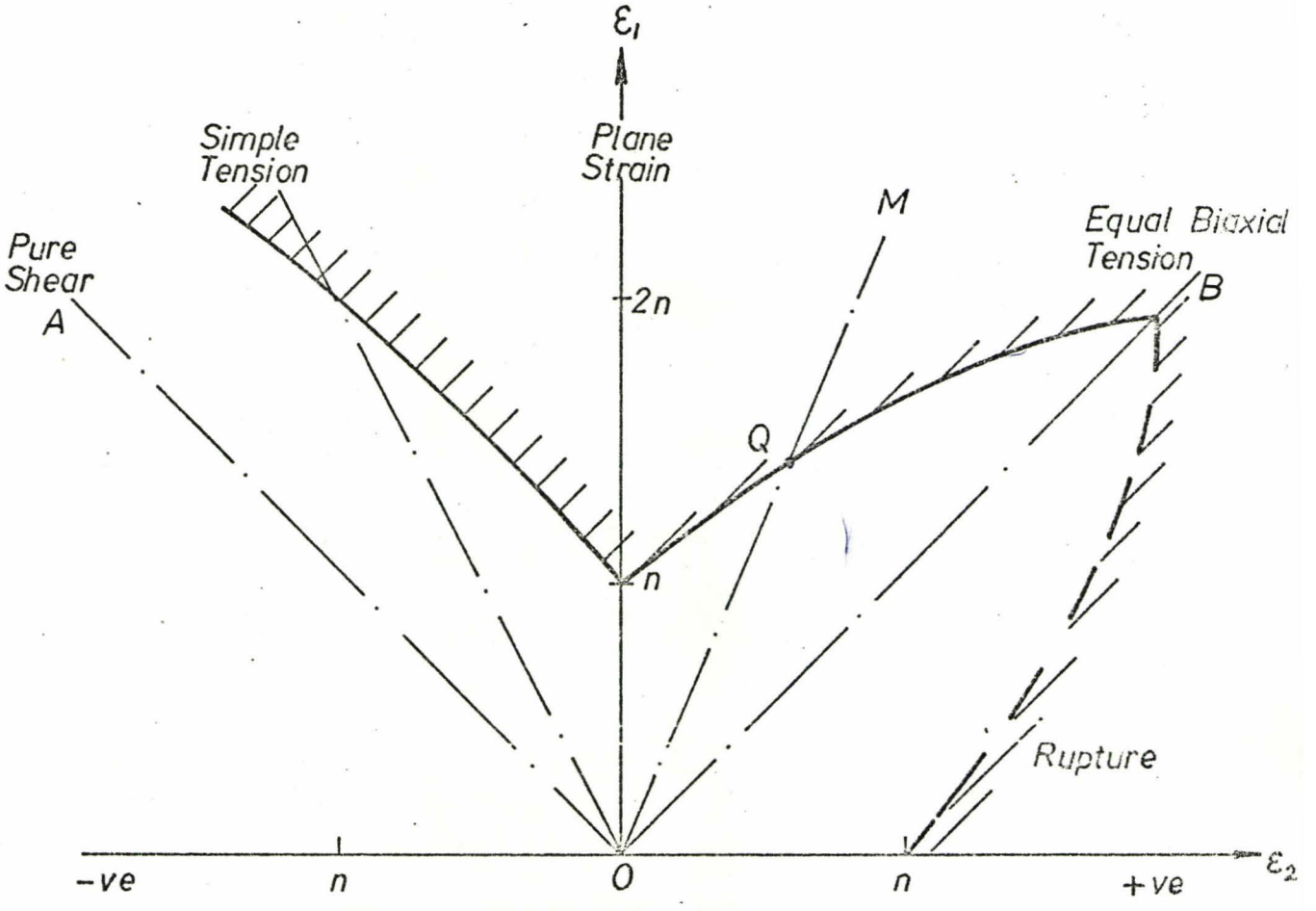

Figure 10.

Forming limit diagram for all regions of deformation in sheet metal forming.
After Sowerby and Duncan (28).

shown in figure 9. The plane strain line OS in this diagram is closer to the equal biaxial tension line OQ than is the case for the isotropic material, R = 1, as shown in Fig. 8 (11). As deformation proceeds, the locus in both cases will expand due to strain-hardening but, as indicated in the diagram, the high R value material is likely to reach failure at an earlier stage.

One would expect that for $R < 1$ as theory predicts that the locus changes from ellipse to a circle as R decreases. However, it was pointed out by Sowerby and Duncan (11) that shortening of the major semi axis for $R < 1$ has never been demonstrated by direct experiment.

Forming limits for a material having low n value determined by Sowerby and Duncan is shown in Fig.10. This diagram applies to all processes in which the ratio of the two strains in the plane of the sheet is reasonably constant. In order to get large strain in the test, the path OA or OB has to be used. In the biaxial test we use path OB. In case of pure shear path OA has to be used - that is performed e.g. in deep drawing a cup. Straining in any process such as along OM is locally stable until the stability envelope is reached at Q. If straining is attempted beyond this, tearing will be expected. Fig. 10 is a diagrammatic representation only, obtained from theoretical curves for

typical values of the parameters. Such curves can be constructed theoretically for any given values of anisotropy, strain hardening and imperfection ratio for a particular sheet.

3. BULGE TEST

3.1 History of the bulge test

In this chapter the author's intention is to give a brief review of some of the work which has led to the present understanding of the process and to the development of metal sheet testing.

It had been observed that in the bulging process, a pressure maximum generally preceded failure (26). This phenomenon, generally called "tensile instability", was investigated for a number of processes by Sachs and Lubahn in 1946. They showed in (12) that the maximum strain at the point of instability depended, among other things, on the geometry of the process and they proposed the development of a general criterion of tensile instability based on the analysis of the stress state and the use of the stress-strain curve for the material in pure tension.

The advantages of the bulging processes as a method for investigating properties of materials at high strain was pointed out by Brown and Sachs in 1948 (13). They proposed that the stress-strain curve obtained in bulging should be equivalent to that obtained in uniaxial tension if the largest true stress for either case is plotted as a function of the greatest natural strain. It so happens that in this case, the result is the same

as that which would be arrived at using the concept of representative stress and strain.

To investigate material behaviour in unequal biaxial stress states, Chow, Dover and Sachs in 1949, bulged specimens in dies having elliptical apertures. They showed that for a given die, strain ratios were closely constant during the processes and that strain states varying between almost uniaxial tension and equal biaxial tension could be obtained by suitable choice of die geometry.

A general analysis of the strain and displacements in the bulging process was given in (14) by Hill in 1950. By employing the assumption that particles on the surface move on trajectories which are circular arcs and orthogonal to the surface of the bulge, he obtained a special solution for the strain and curvature in terms of the ratio of bulge height to die radius. Applying this solution to a material whose stress-strain relationship could be fitted by a function $\bar{\sigma} = A\bar{\varepsilon}^n$, where $\bar{\sigma}$ and $\bar{\varepsilon}$ denote representative stress and strain as defined below, he obtained the result that the instability thickness strain ε^* was given by the expression

$$\varepsilon^* = 4(2n + 1)/11 \qquad (3.1.1)$$

This analysis agreed with the observed fact that even for materials exhibiting very little strain-hardening, ε^* was

generally at least equal to about 0.4 (26).

A carefully executed and extensive investigation of the bulge process was performed by Mellor in 1956 as described in (15). This work was instituted by the late Professor Swift in the expectation that the bulge test would simulate the strain development and distribution over the head of hemispherical punch in the simple hemispherical deep-drawing operation. Mellor investigated the strain distribution and geometry of the bulge for a wide variety of materials. He showed that a good correlation could be obtained for most materials between the stress-strain curve obtained from the bulge test and that obtained by combined rolling and simple tension test.

Previous work on the investigation of the effect of anisotropy on the bulge process has already been reviewed by Mellor and Bramley in (16) who, in the same work, present the results of tensile and bulge tests for a particular anisotropic steel. The parameters characterizing anisotropy as proposed by Hill (17) were determined from the tensile tests, and using an average value of R (defined differently to that given in equation 2.1.9) they were able to predict quite closely the stress-strain curve obtained in the bulge test. Preliminary information about the effect of the strain-rate on the stress-strain curve obtained from the bulge test was also given in this work.

A general method of analysing axisymmetric sheet metal forming using the incremental strain theory has been developed by Woo in 1964 (18). This method involves the use of an experimentally determined stress-strain curve and successive approximations of stresses and strains in the material. Solutions have been obtained for the bulge process by use of a digital computer and good agreement obtained between experimental and theoretical results for pressure, strain, and curvature in the process.

To determine the representative stress-strain curve from the bulge test, Mellor (15) scribed a number of concentric circles on the specimen and measured the diameters of the circles with a travelling microscope after each increment in hydrostatic pressure. The polar strain was then determined by plotting the circumferential strain against initial radius of the circle and extrapolating to zero radius. Similarly, the polar radius of curvature was obtained by extrapolation of spherometer readings. This method gives accurate results but is too time-consuming for frequent use.

The fast method of determining the stress-strain curve from the bulge test was suggested by Duncan and Johnson (19). They designed an extensometer and spherometer and on the basis of the readings obtained, the stress-

strain curve could be determined. An autographic unit was also designed (24) and (25) at Manchester University but this has not attracted much attention.

3.2 The desirable features of the bulge test.

There are a very large number of possible loading or stress systems which could be used to deform sheet metal for the purpose of testing it to obtain its fundamental stress-strain curve. The desirable features pointed out by Johnson and Duncan in (27) which any such test method should possess are:

i) Test specimens should be easily prepared and their performance not influenced by small differences in the workshop techniques used in their preparation.

ii) The test should be capable of being performed using simple mechanical apparatus. The construction of the testing apparatus should be able to be completely specified so that nominally identical testing machines give identical results.

iii) The greatest value of the representative strain obtainable should be as far as possible, at least equal to that occurring in the industrial processes in which the material will be used.

iv) The results of the test should be expressed in the form of a curve rather than by a single parameter.

v) The curve obtained should be a fundamental material property, and independent of the specimen size and the imposed stress systems.

vi) The computation of any results required should be minimal.

vii) Where the material is liable to exhibit anisotropy, the strain system in the test should be similar to that in the industrial process.

Unfortunately, no one test is likely to satisfy all seven requirements.

In the tensile test a specimen can be prepared easily, although care must be exercised in machining the uniform width and the radii at the shoulders to be gripped. That is a rather time-consuming operation. The hardened zone caused by the blanking operation must be removed. It is easy to compute the true stress - strain curve from this test and the testing apparatus is simple. Its principal defect is that for materials exhibiting a low degree of work hardening (e.g. hard aluminum) the maximum strain in the tensile test is much less than that occuring in many

industrial processes.

The bulge test fulfills not all but most of the requirements for the test method mentioned earlier. The test specimen is a simple circular blank, and because measurements are only taken over a central portion, the results cannot be influenced by the methods used to cut out the blanks. The test equipment is mechanically simple as indicated in the next chapter, and the results are repeatable from one test apparatus to another because the load is applied directly by hydrostatic pressure and friction effects are non-existent.

3.3 Information to be derived from the bulge test

The true stress-strain curve for the material can be obtained from measurements of curvature and extension at the pole and bulging pressure.

The maximum strain at fracture was considered to be an important metal forming parameter by Sachs (20) and this can be readily determined from a measurement of final thickness.

While the variation of polar height of the bulge with bulging pressure can be measured during the test it is not clear how this information should be interpreted. It has been shown (21) that there is some correlation between maximum bulge height and strain-hardening index but the determination of the stress-

strain relation from bulge height and pressure measurements using Hill's special theory does not always give accurate results (Ref.26).

3.4 Determination of the true stress-strain curve from the bulge test

The profile of a bulged specimen has been shown by experiment to be spherical in the polar region so that the membrane stress at the pole is

$$\sigma = \frac{p\,\rho}{2t} \qquad (3.4.1)$$

Where:

p - hydrostatic pressure

ρ - radius of curvature

t - current thickness

By symmetry, the stress is uniform in all directions and as the stress normal to the surface is negligible, the principal stresses are:

$$\sigma_1 = \sigma_2 = \sigma \qquad \sigma_3 = 0 \qquad (3.4.2)$$

The circumferential strain around a circle concentric with the pole is

$$\varepsilon = \log_e \frac{D_1}{D_o} \qquad (3.4.3)$$

Where:

D_o - initial diameter

D_1 - current diameter

ε - natural or Logarithmic strain

When D_o becomes vanishingly small, equation (3.4.3) gives the strain at the pole which, by symmetry, is uniform in all directions.

The principal strains at the pole are:

$$\varepsilon_1 = \varepsilon_2 = \varepsilon \quad \text{and} \quad \varepsilon_3 = \varepsilon_t \qquad (3.4.4)$$

From the condition of incompressability

$$\varepsilon_t = -2\varepsilon \qquad (3.4.5)$$

The current thickness at the pole, t, can be obtained from the measured strain and the original thickness t_o since

$$\varepsilon_t = -2\varepsilon = \log_e \frac{t}{t_o} \qquad (3.4.6)$$

The representative stress $\bar{\sigma}$ and representative strain $\bar{\varepsilon}$ may be defined as:

$$\bar{\sigma} = \left\{\tfrac{1}{2}\left[(\sigma_1 - \sigma_2)^2 + (\sigma_2 - \sigma_3)^2 + (\sigma_3 - \sigma_1)^2\right]\right\}^{\frac{1}{2}} \qquad (3.4.7)$$

$$\bar{\varepsilon} = \frac{\left\{2\left[(\varepsilon_1 - \varepsilon_2)^2 + (\varepsilon_2 - \varepsilon_3)^2 + (\varepsilon_3 - \varepsilon_1)^2\right]\right\}^{\frac{1}{2}}}{3} \qquad (3.4.8)$$

Using stress and strain defined in this manner, it has been shown that a single stress-strain curve will be valid for all processes, providing that in the process the strain-ratios remain constant and the directions of the principal axes of successive strain increments do not alter. Using equations (3.4.7) and(3.4.8) it may be shown that in the tension test $\bar{\sigma}$ and $\bar{\varepsilon}$ are equal to the uniaxial true stress and natural strain and in the bulge test

$$\bar{\sigma} = \sigma \quad \text{and} \quad \bar{\varepsilon} = 2\varepsilon \qquad (3.4.9)$$

The stress-strain curve can be obtained by using a biaxial test extensometer. It is assumed that in the region over which measurements are taken (equal to a circle at the initial radius of about 0.6 in.) the strain and curvature are uniform and equal to the values at the pole. Two mutually perpendicular views are shown in Fig.12 and 13 and the operation is evident from these figures, although detail description is given in chapter 4 to which the reader is referred.

Tables can be prepared as shown in appendix B which will enable the parameters $\overline{\varepsilon}$ and ς and the thickness ratio t_o/t to be determined directly from the dial gauge readings. The stress $\overline{\sigma}$ can be calculated from equation (3.4.1):

$$\overline{\sigma} = \frac{P\varsigma}{2t}$$

4. THE BULGING EQUIPMENT

The bulging equipment designed by the author was manufactured mainly under his supervision in the McMaster University machine shop.

The individual parts of this equipment are described in detail below.

4.1 The Bulging Die

Circular specimens were bulged in the die shown in Fig. 11. The specimen placed in the die was clamped initially between the die ring, 2, screwed into the body of the die and the clamping ring. Since that initial clamping is not sufficient to grip the specimen, the hydrostatic pressure supplied by a hand pump is imposed on the under face of the clamping ring giving required clamping pressure. Special care is taken to make sure that there is no air trapped in the hydraulic system. When sufficient clamping is achieved the clamping valve is shut off and the hydrostatic pressure starting from zero is imposed on one side of the specimen causing bulging. As the bulging pressure begins to rise, the clamping valve can be opened so that equal pressures exist under the blank and under the clamping ring. The die described above has a 6" hole. Detail description of the bulging operation is given in appendix A.

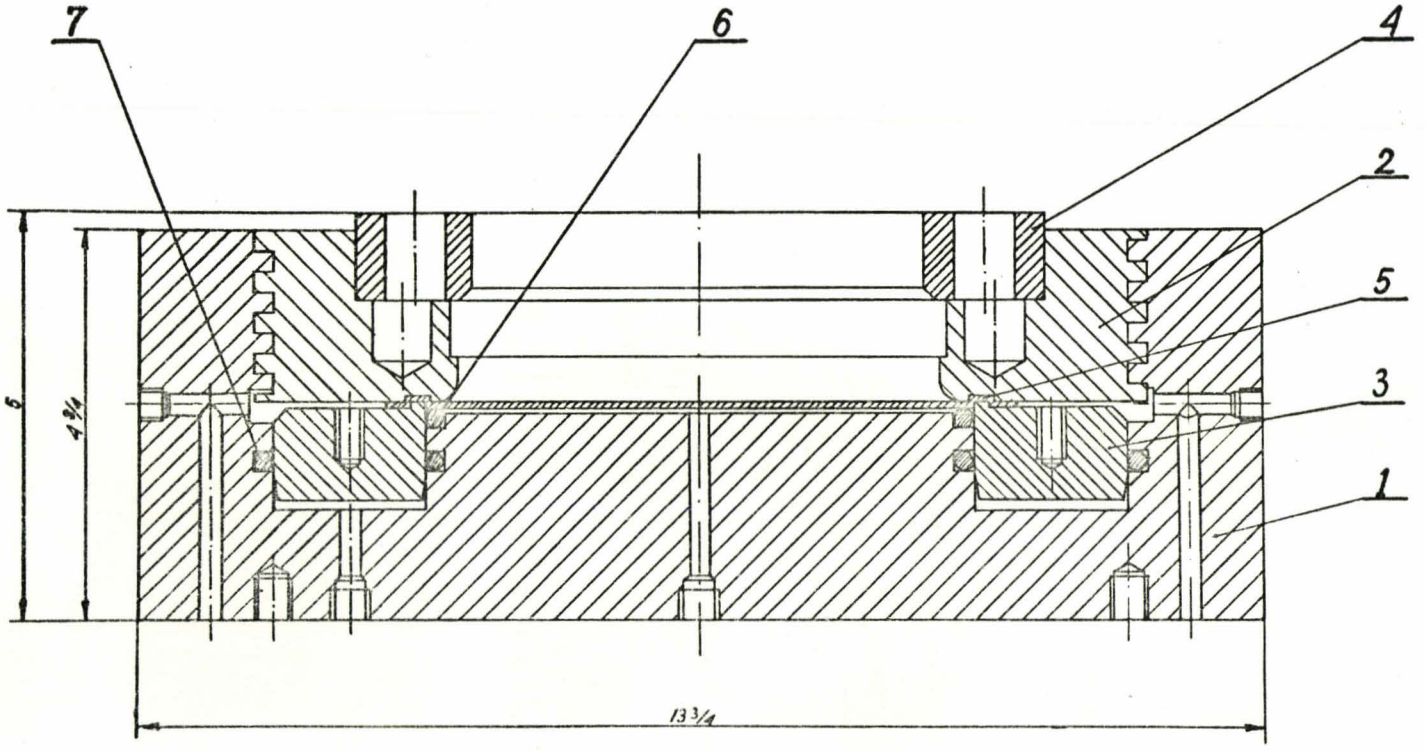

7	NITRILE	O-RING 2-450 1/4	N219-7
6	NITRILE	O-RING 2-438 1/4(2)	N219-7
5		SPECIMEN 6" dia	
4	MS	LOCATING RING	D.0104
3	MS	CLAMPING RING	D.0103
2	MS	NUT	D.0102
1	MS	DIE BASE	D.0101
PART NO.	MATERIAL		DRAWING NO.

Bulging die assembly		DRAWING NO. D.0100
Mechanical Eng'g	DIMENSIONS IN INCHES	SCALE: FULL SCALE
McMaster University	P. H. Albertin	
Hamilton, Ont		DATE: JUNE 4, 1971

Figure 11. Bulging die.

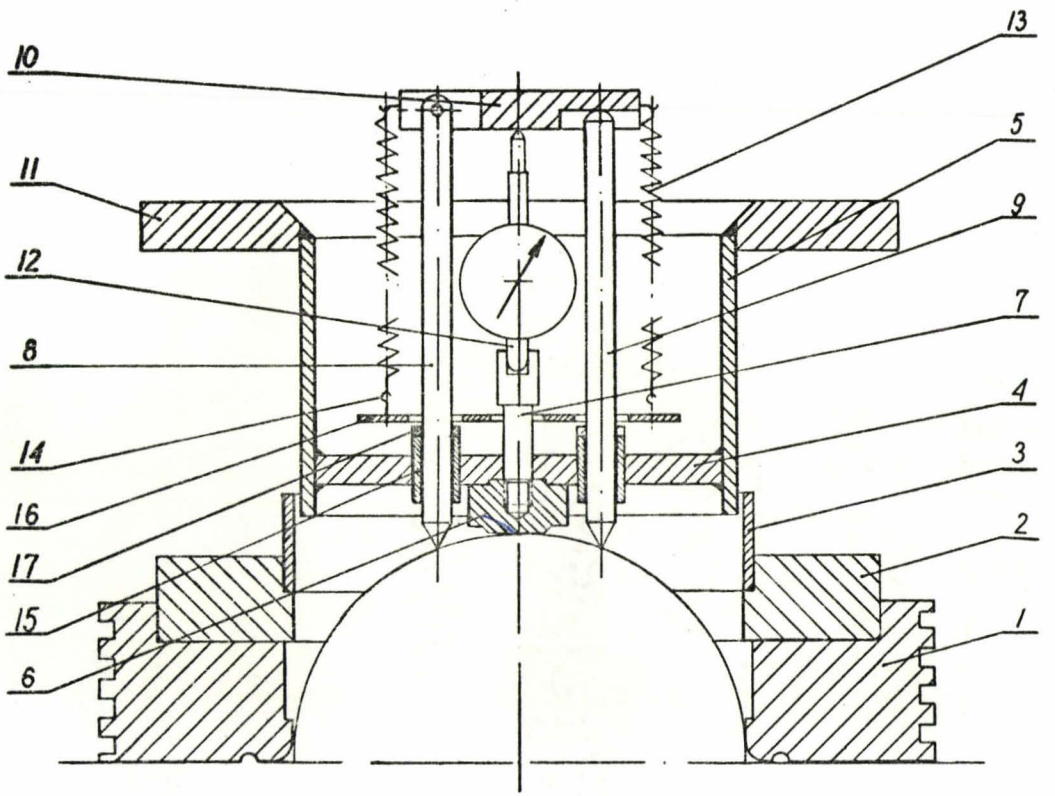

17	BRASS	RETAINNING RING (2p)	S 0115
16	MS	PLATE	
15	BRASS	BUSHING (2p)	S 0115
14		HOOK (4p)	
13		SPRING (2p)	
12		GAUGE	
11	ALUM	CARRYING PLATE	E 0108
10	MS	MEASURE PLATE	S0115
9	GR STOCK	PIN	S 0115
8	GR STOCK	PIN	S 0115
7	MS	SCREW	S 0105
6	MS	SQUARE	E 0103
5	ALUM	RING	E 0108
4	ALUM	SHIELDING PLATE	E 0108
3	ALUM	SHIELDING RING	E 0102
2	MS	RING	D. 0104
1	MS	NUT	D. 0102
PART NO	MATERIAL		DRAWING NO

Spherometer	DRAWING NO. S 0200
Mechanical Engg (DIMENSIONS IN INCHES)	SCALE FULL SCALE
McMaster University	P.H. Albertin
Hamilton, Ont.	DATE NOV. 23rd, 1971

Figure 12. Spherometer.

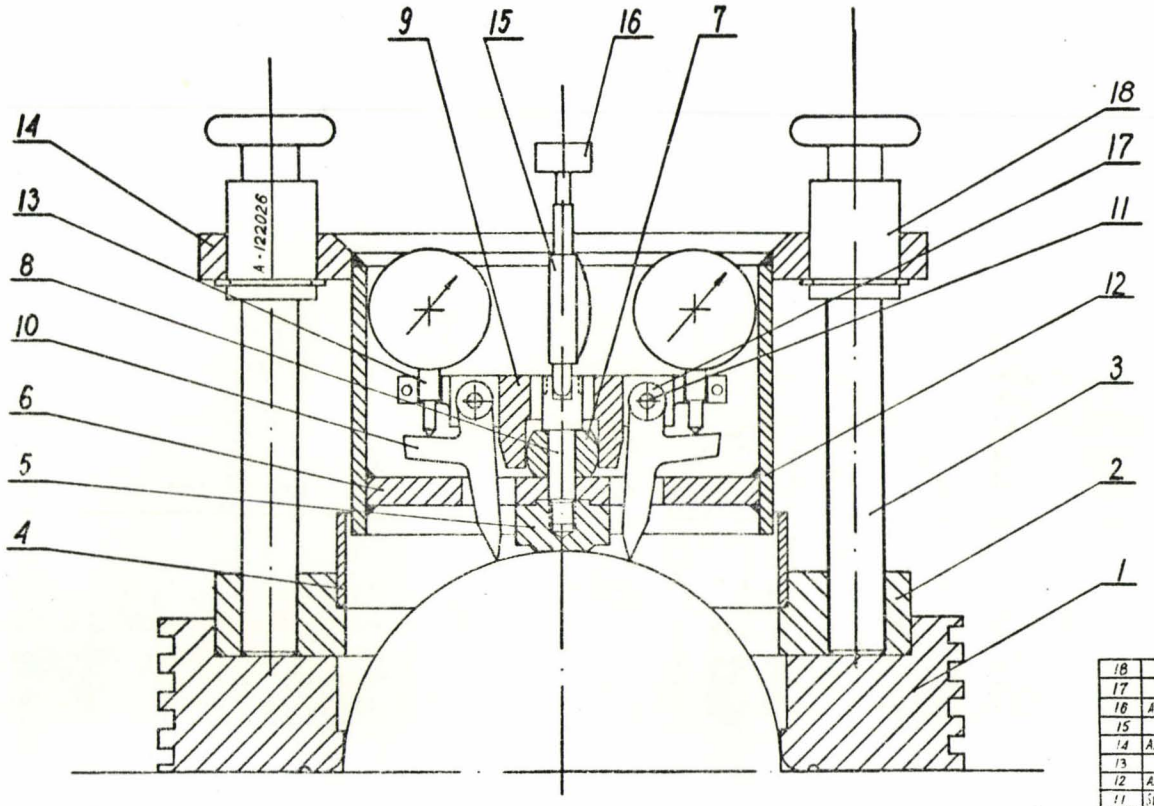

PART NO	MATERIAL		DRAWING NO
18		3/4 BALL BUSH NG (2p)	A-122026
17		PRECISION BALL BEARI. SLIDE	E 1-6
16	ALUM	MEASURE PLATE	S. 0105
15		GAUGE	
14	ALUM	CARRYING RING	E 0108
13		GAUGE (2p)	
12	ALUM	RING	E. 0106
11	St Steel	DOWEL (2p)	A 5-25
10		LEG	E 0105
9	ALUM	LEGS GUIDER	E 0107
8	ALUM	SCREW	S. 0105
7	ALUM	PIVOT BLOCK	E 0103
6	ALUM	SHIELDING PLATE	E 0108
5	MS	GAUGE BLOCK	E 0103
4	ALUM	SHIELDING RING	E 0102
3	MS	GUIDE PIN (2p)	E 0101
2	MS	RING	D 0104
1	MS	NUT	D 0102

Extensometer		DRAWING NO. E 0100
Mechanical Eng'g	DIMENSIONS IN INCHES	SCALE FULL SCALE
McMaster University	P. H. Albertin	
Hamilton, Ont.		DATE JULY 8th, 1971

Figure 13. Extensometer.

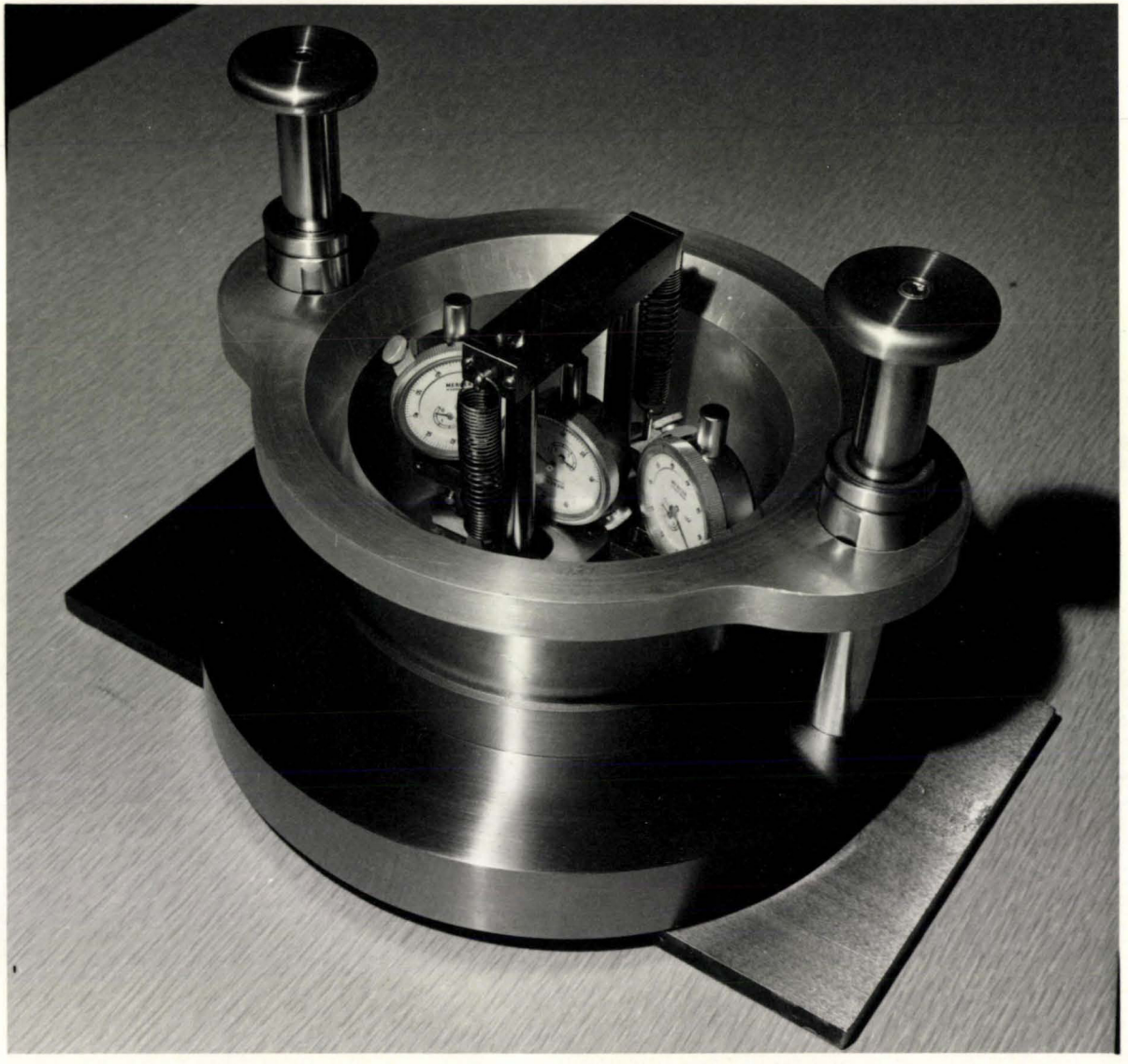

Figure 14. Biaxial test unit - extensometer, spherometer.

4.2 The Biaxial test unit: Extensometer, Spherometer

The biaxial test unit consists of the extensometer and the spherometer. Both instruments are combined in one unit working in two mutually perpendicular planes (Fig.14).

The extensometer is an instrument for measuring extension and the spherometer for measuring of the curvature at the centre of a circular diaphragm which is deformed in the hydrostatic bulge test.

The unit rests on the surface of the specimen and is guided by two columns fixed in the locating ring, 2, shown in Fig.13.

While hydrostatic pressure is applied to one side of the specimen deforming it to a symmetrical dome the unit slides freely on the vertical columns and instrument probes follow the path of the bulging specimen.

A gauge block 5, Fig.13 ensures that the probes of the extensometer are initially a constant distance apart. The movement of the probes is registered on the two outside gauges and extension is derived from their sum. The pivot block, 7, ensures that both probes are in contact with the specimen, even if there is some slight eccentricity in the dome. Two springs provided at the ends of the measure plate, 16, Fig.12 ensure that the extensometer is not resting all its weight on the probe tips.

The operation of the spherometer can be seen from Fig.12. The two pins of the spherometer can slide in the bushings, and the relative movement is registered on the central dial gauge, so that the radius of curvature can be calculated from this reading. The arrangement of pins and the measure plate were designed to ensure that both pins are in contact with the specimen even if there is some slight eccentricity in the dome. The true stress - strain curve for the diaphragm material can be computed from the extensometer and the spherometer readings.

Value of the true stress and the strain were calculated on a computer CDC6400 and magnitudes plotted on a graph as shown in appendix D.

4.3 Hydrostatic test bench

The bulging die is mounted on a general purpose hydrostatic test stand as shown schematicly in Fig.15. The circuit is built with commercially available hydraulic components. All fittings used in a system were manufactured by Swagelok. Tubing used is 3/8" DIA.

Required pressure is delivered by a hand operated pump "Enerpac" model P51 and three Webster pressure gauges are used to permit pressure readings in the range $5 \div 5000$ lb/in^2.

The hydraulic system as shown schematically in

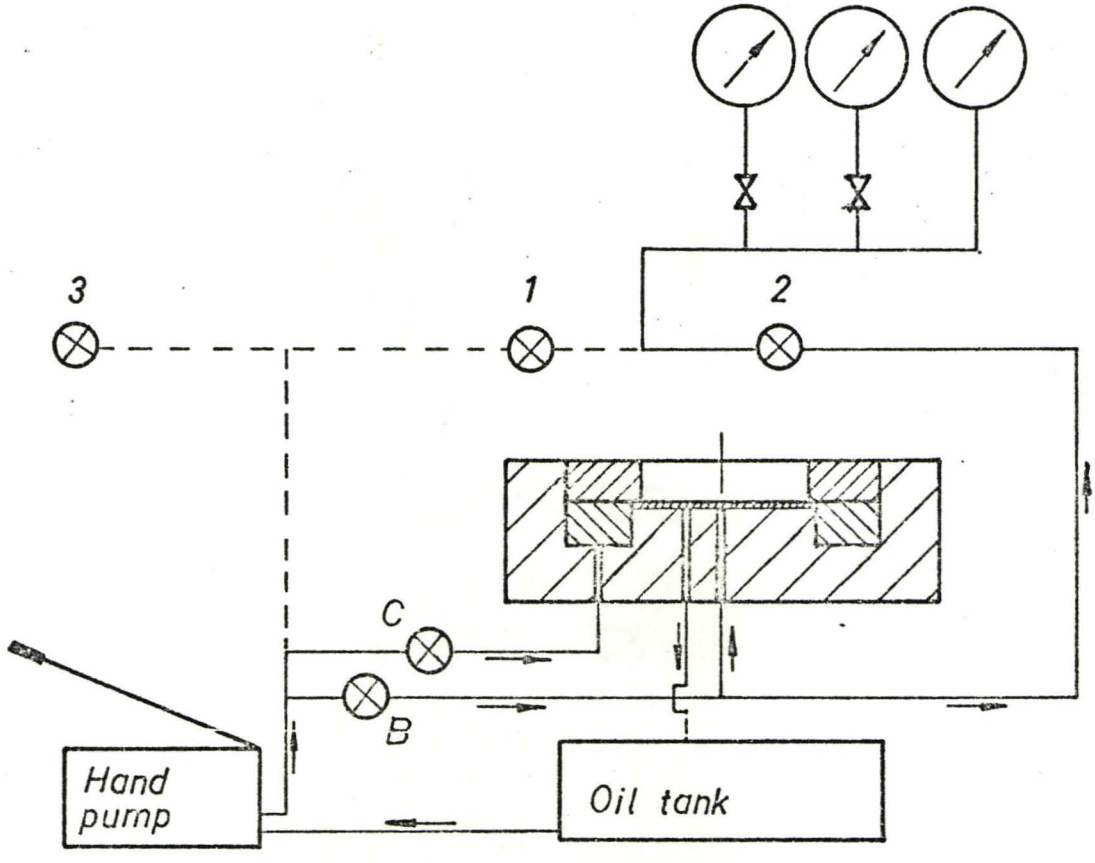

B - Bulging valve
C - Clamping valve

Figure 15.

Hydraulic system

Fig.15 has introduced two additional valves N^{o} 2 and N^{o} 3 which allow to use the same hydraulic system for the elliptical dies (not described in this thesis, since it is not in the scope of this experiment).

5. EXPERIMENTS

Two kinds of experiments are performed: tensile test and hydrostatic bulging of a circular diaphragm.

Comparison of both of them is done by plotting representative stress-strain curves.

The experiment was carried out with two materials - mild steel and aluminium.

The biaxial bulging test unit was calibrated before being used in the hydrostatic bulging experiment. A description of the calibration is given in appendix C.

5.1 Specimens preparation

(a) Tensile test

Specimens as shown in Fig.16 were taken in three various directions 0°, 45°, 90° degrees with respect to the rolling of the sheet. Special care was taken during the machining operation so that all specimens had uniform width all the length.

(b) Bulge test

The shape of the specimens as shown in Fig.17 does not require any particular preparation as long as the specimen is approximately of 8.5" DIA. Rolling direction is marked throughout the centre of the specimen so that the extensometer could be placed in three various directions 0°, 45°, 90°, with respect to the rolling direction.

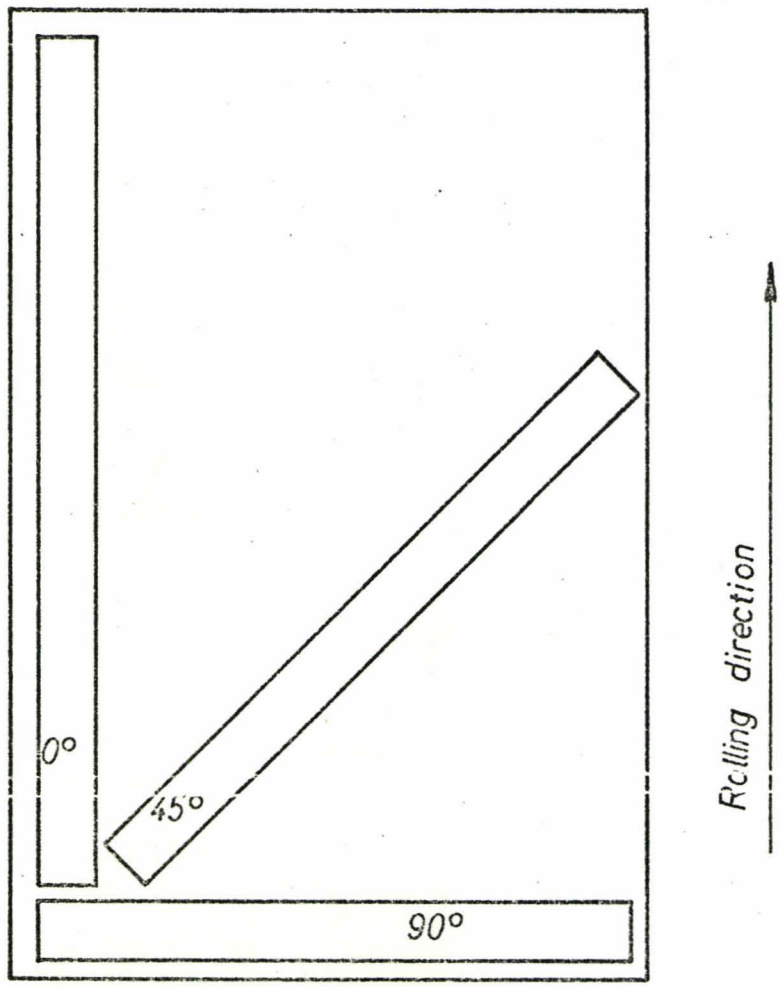

Figure 16.

Tensile specimens in three different directions with respect to the rolling direction of the metal sheet.

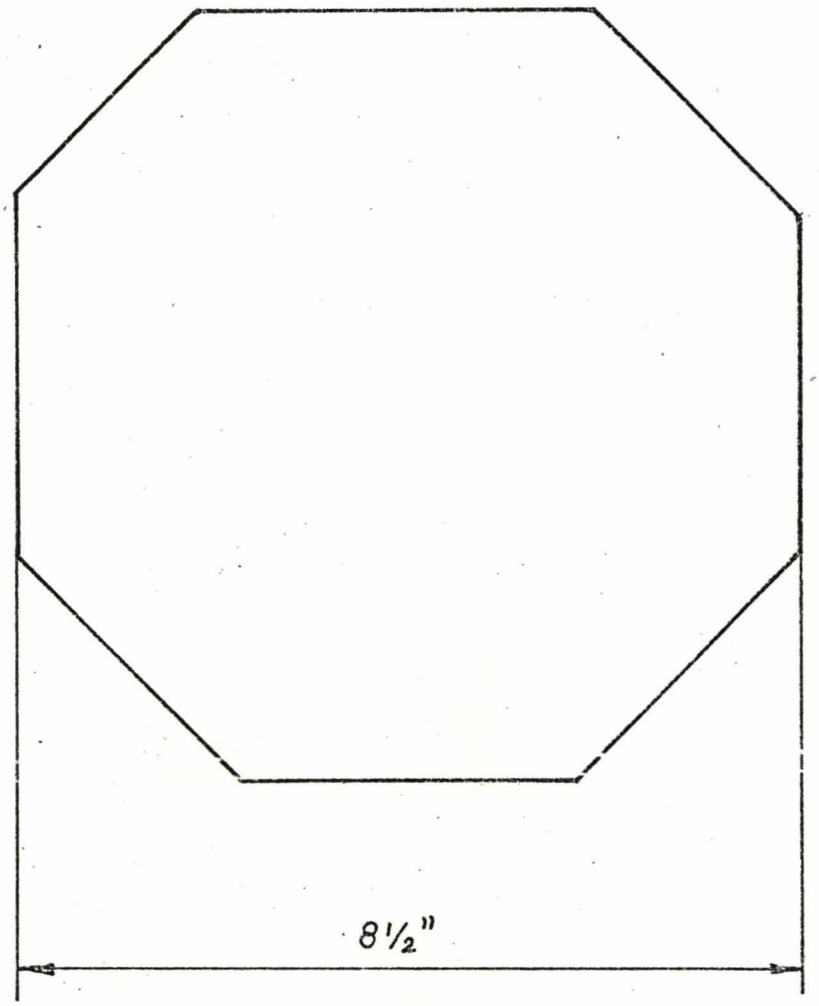

Figure 17.

Bulge specimen

5.2 Testing procedure

(a) Tensile test

The gauge length 2" is marked on the specimen (marked by an arrow on Fig.25) and the original width and thickness is measured. Next the specimen is clamped on the jaws of the test machine "Tinius Olsen". The load is read at 2.05", 2.10", 2.20", 2.30", 2.40", 2.60", 2.80" - distances of the gauge marks.

When the specimen reaches 20% elongation (2.40") the test is stopped and the specimen unloaded. The width of the specimen at the gauge marks and at the centre between the two gauge marks is taken, and exact gauge marks distance is measured.

Next the specimen is reloaded and the load readings are taken until the specimen failure occurs. Computation is done with an assumtion that tested specimen has uniform cross-section area A and is subjected to a tensile force P, therefore, applied stress is:

$$\sigma_1 = \frac{P}{A} \qquad (5.2.1)$$

where

$$A = t * w \qquad (5.2.2)$$

t - current specimen thickness

w - current specimen width

If l_o is the original gauge length, and l is the current

gauge length, the volume of the specimen between the gauge marks is:

$$l_o \quad w_o \quad t_o = l \quad w \quad t \qquad (5.2.3)$$

where: w_o - original width

t_o - original thickness

Combining (5.2.2) and (5.2.3) and substituting into (5.2.1)

$$\sigma_1 = \frac{P \quad l}{l_o \quad w_o \quad t_o} \qquad (5.2.4)$$

For large deformations, logarithmic strain is a better indication of strain than the engineering strain, in this case the strain given by:

$$\varepsilon_1 = \ln \frac{l}{l_o} \qquad (5.2.5)$$

To take into account the various stress and strain system representative stress and representative strain are introduced:

$$\bar{\sigma} = \frac{1}{\sqrt{2}} \{(\sigma_1-\sigma_2)^2 + (\sigma_2-\sigma_3)^2 + (\sigma_3-\sigma_1)^2\}^{\frac{1}{2}} \qquad (5.2.6)$$

$$\bar{\varepsilon} = \frac{\sqrt{2}}{3} \{(\varepsilon_1-\varepsilon_2)^2 + (\varepsilon_2-\varepsilon_3)^2 + (\varepsilon_3-\varepsilon_1)^2\}^{\frac{1}{2}} \qquad (5.2.7)$$

where: σ_1, σ_2, σ_3 - principal stresses

ε_1, ε_2, ε_3 - principal strains

Since for uniaxial tension

$$\sigma_2 = \sigma_3 = 0 \qquad \text{and}$$

$$\varepsilon_1 = -\tfrac{1}{2}\varepsilon_2 = -\tfrac{1}{2}\varepsilon_3$$

Representative stress and representative strain can be expressed by:

$$\bar{\sigma} = \sigma_1 \tag{5.2.8}$$

$$\bar{\varepsilon} = \varepsilon_1 \tag{5.2.9}$$

The value $\bar{\sigma}$ and $\bar{\varepsilon}$ were plotted on a graph as shown on Fig.21.

(b) Hydrostatic Bulging

The thickness of the specimen is measured before it is loaded into the die. Every time before bulging, special care is taken to ensure that there is no air in the hydraulic system. After sufficient clamping is achieved, the biaxial test unit (with previous gauges set to zero) is placed into the locating ring onto the die. Three different instrument location 0°, 45°, 90° with respect to the rolling direction of the metal sheet are investigated. Detail operation instruction for bulging experiment are given in appendix A where reader is referred.

Pressure is applied by means of the hand pump

and before taking a reading pressure is held constant for a few seconds and read; it may be allowed to fall off while the dial gauges are read.

Readings of the pressure, two extensometer gauges and the spherometer gauge are taken approximately every .005" indicated on each of the extensometer gauges.

Using the assumption that the addition of a hydrostatic stress system does not influence yielding as it was shown by Johnson and Duncan in (19) the stress system in the polar region in the hydrostatic bulge test is equivalent to a uniaxial compressive stress normal to the surface of the material. Thus the uniaxial stress - strain curve is obtained by plotting the membrane stress against the thickness strain ε_t as equation (3.4.9).

Bulging is performed until failure of the specimen occurs.

Typical hydrostatic bulge result for a mild steel is presented in appendix D.

In order to check the accuracy of the representative stress - strain curve obtained by means of the bulge test unit, an additional test was performed.

A number of circles from 3/4" to 4" DIA in steps 0.5" were scribed on a bulge specimen as shown in Fig.18.

Readings of the diameter extensions were taken and the difference in height between the pole and the

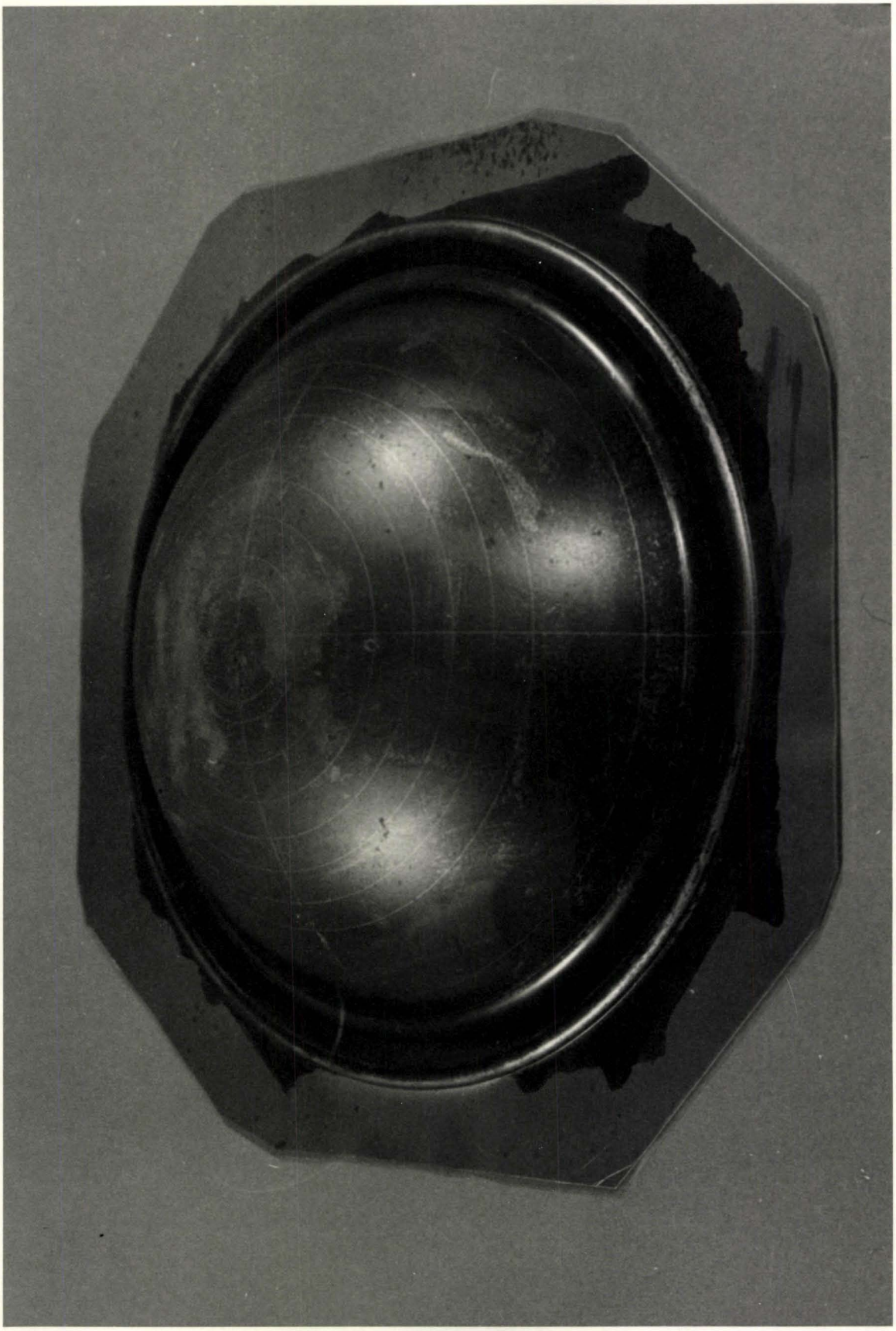

Figure 18. Gridded specimen.

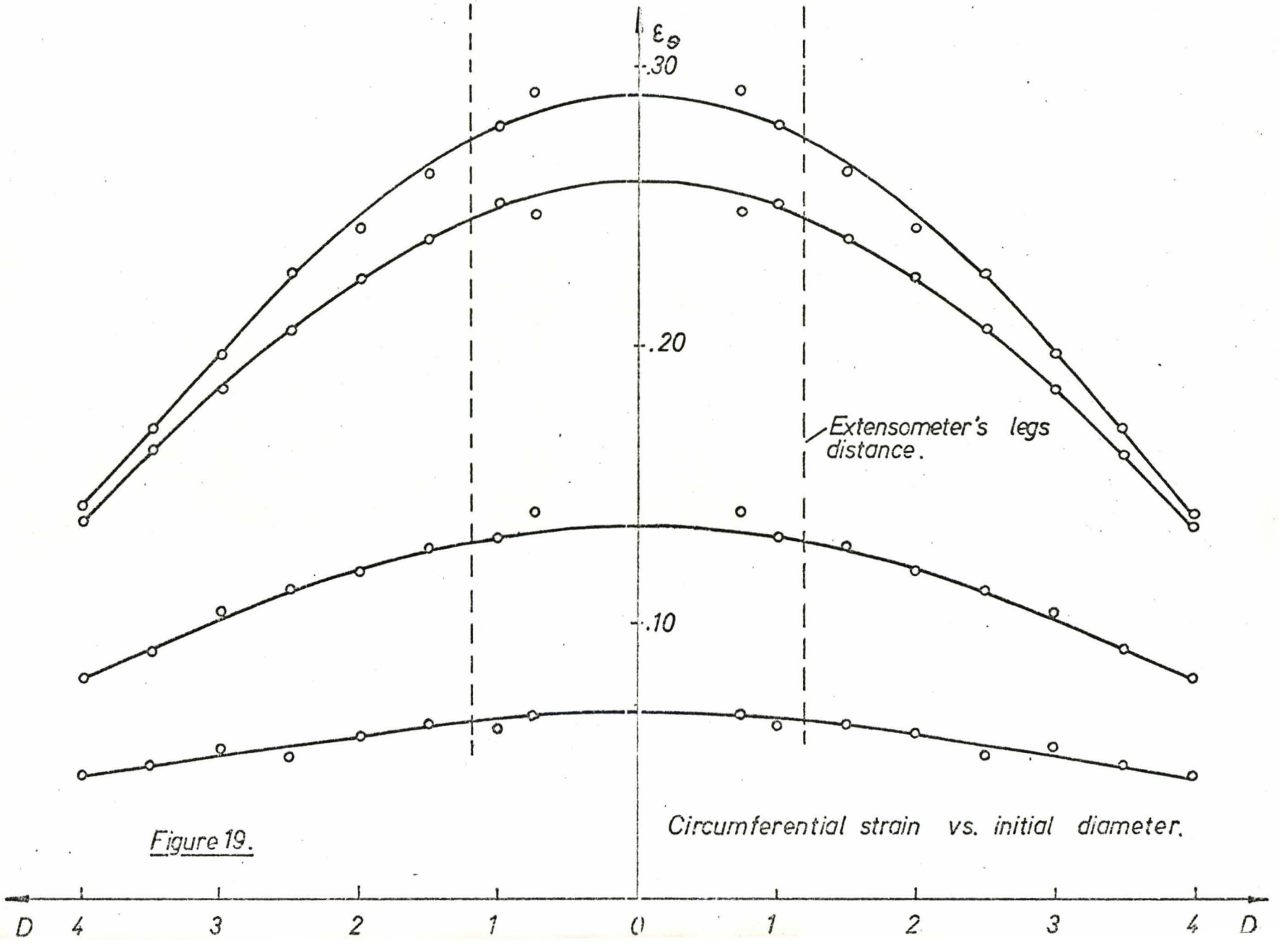

Figure 19.

Circumferential strain vs. initial diameter.

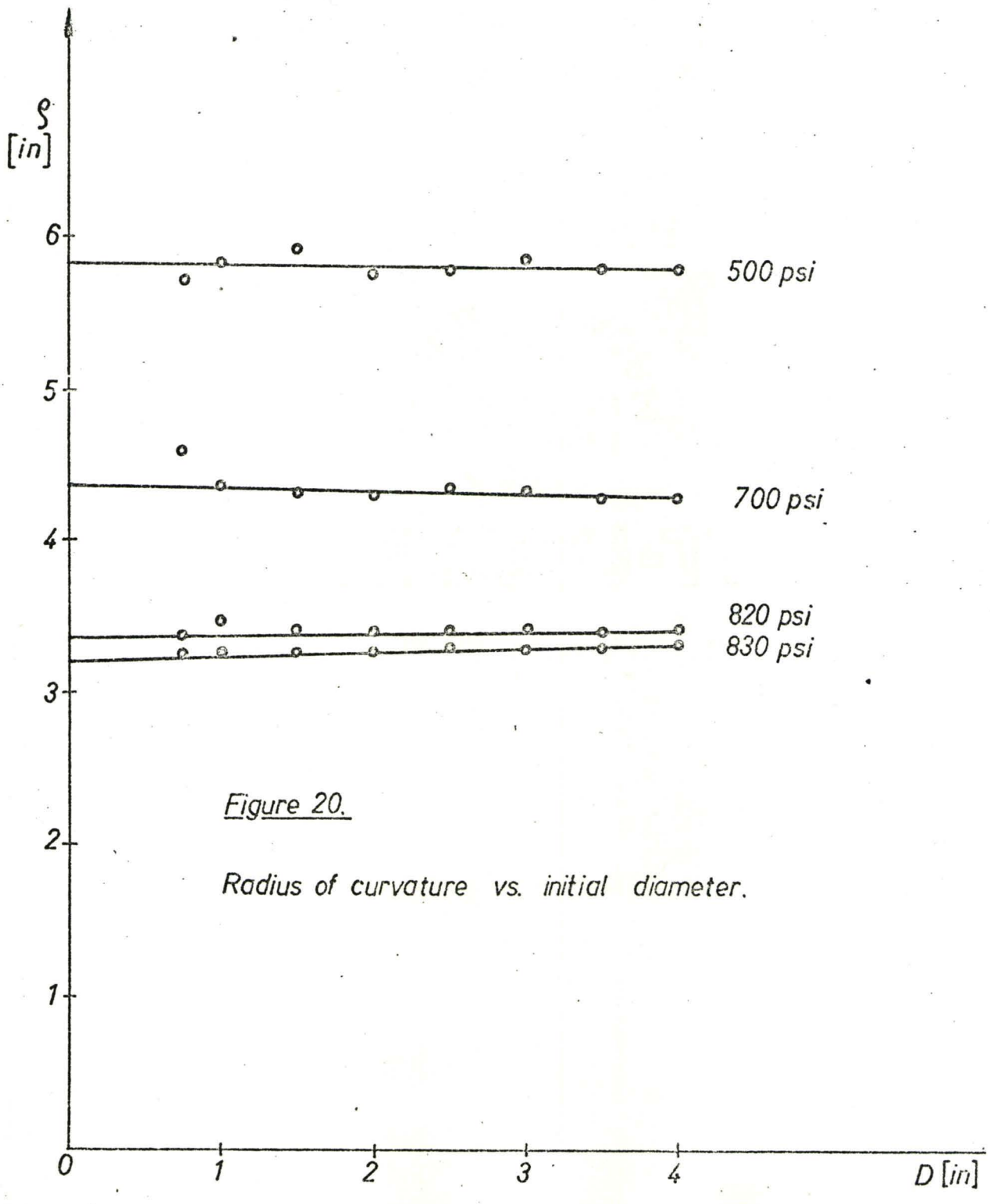

Figure 20.

Radius of curvature vs. initial diameter.

scribed circles were measured for various pressures. The data so obtained was used to calculate hoop strain and radius of curvature calculations, and finally plotted versus the initial diameter scribed on a bulge specimen Fig.19 and Fig.20.

To check how large the error is in representative stress - strain curve due to the finite distance over which extension and curvature is measured, the polar values of ε_θ and ρ (Fig.19 and Fig.20) were found by extrapolation to zero radius and $\bar{\sigma}$ and $\bar{\varepsilon}$ was calculated for these values (Fig.21).

6. RESULTS

A typical bulge test curve for mild steel sheet (.030 thickness) and a comparison with tensile test is presented in Fig.21.

Three tensile curves shown below in the diagram correspond to test on specimens in three varying directions with respect to the rolling direction of the sheet.

There is a significant difference between the tensile and the bulge test result; this can probably be explained to some extent by the anisotropic behaviour of the material.

The average value of normal anisotropy in the sheet tested was $\bar{R} = 1.416$.

On a base of the tensile results, a theoretical bulge curve was calculated using the formula suggested by Bramley and Mellor in (2):

$$\bar{\sigma} = \left[\frac{1 + \bar{R}}{2}\right]^{\frac{1}{2}} \sigma_{T}\text{ave} \qquad \bar{\varepsilon} = \left[\frac{2}{1 + \bar{R}}\right]^{\frac{1}{2}} \varepsilon_{T}\text{ave} \quad (6.1)$$

As can be noticed there is certain discrepancy between the theoretical and experimental bulge test results in Fig.22. Previous work (Bramley and Mellor) showed a similar, but smaller discrepancy. In this calculation an average **R** value was used, while in Ref.2, the calculation was based on a tensile test for that orientation in which **R** was equal to the average value.

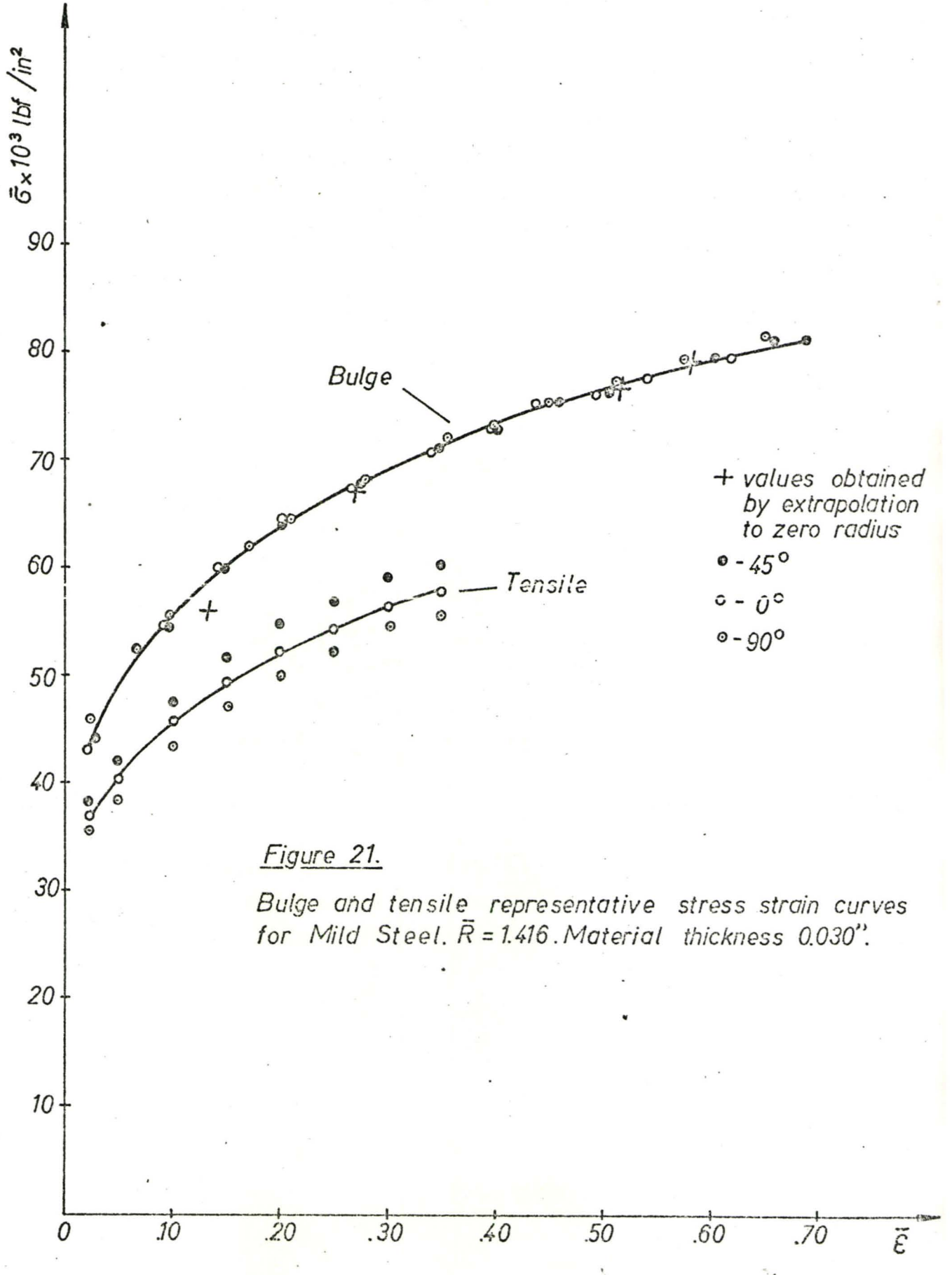

Figure 21.

Bulge and tensile representative stress strain curves for Mild Steel. $\bar{R} = 1.416$. Material thickness 0.030".

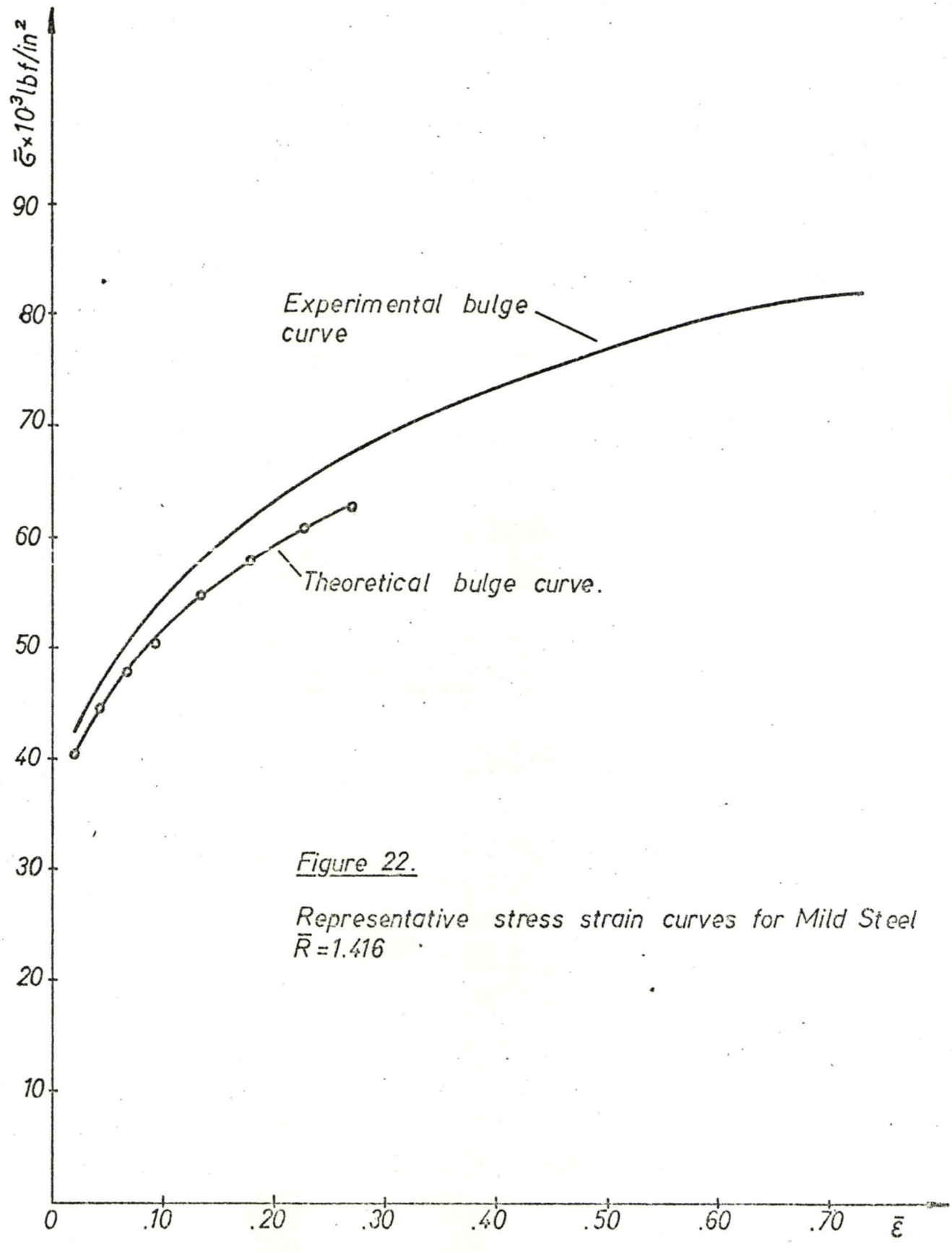

Figure 22.

Representative stress strain curves for Mild Steel $\bar{R} = 1.416$

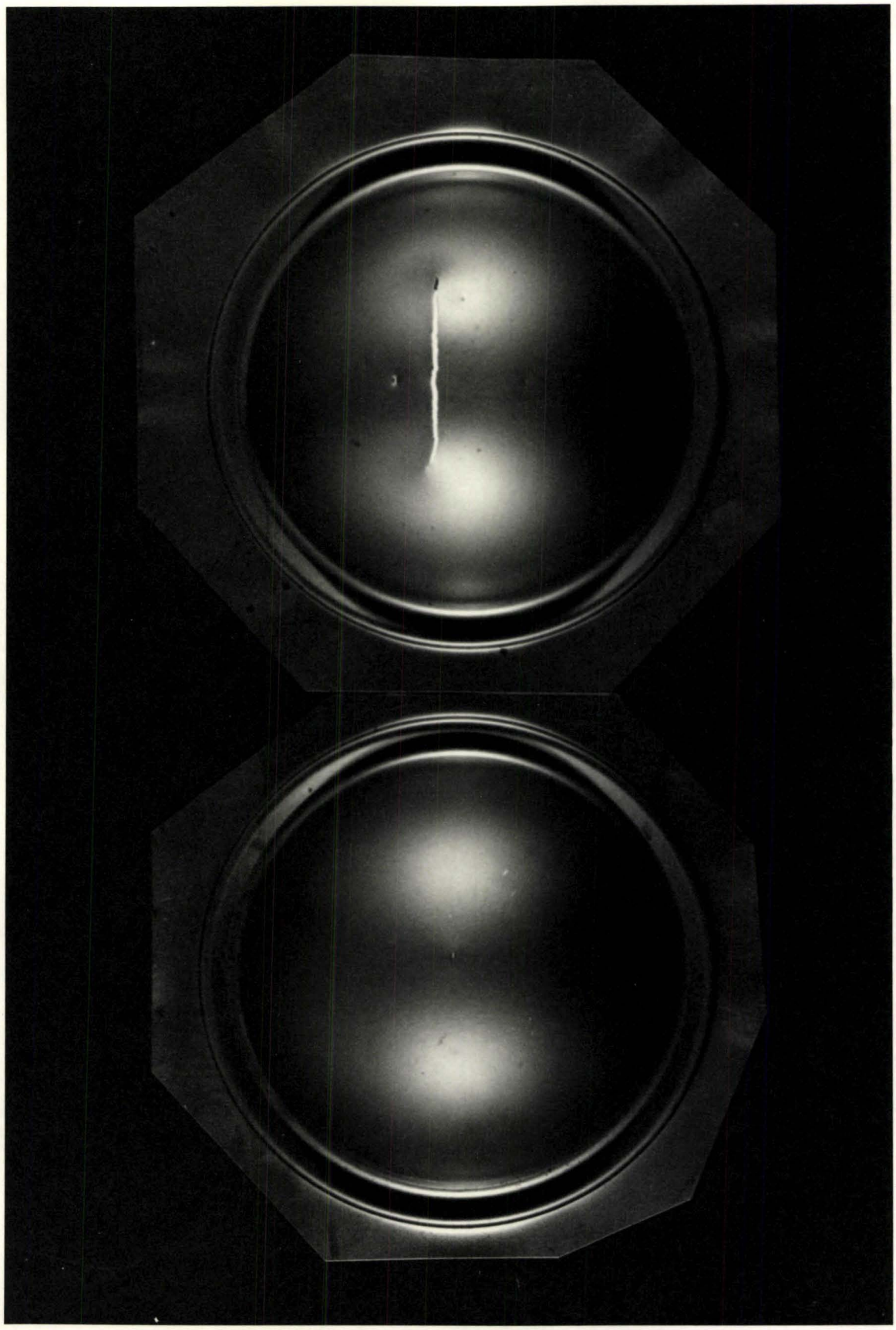

Figure 23. Failure specimen (mild steel).

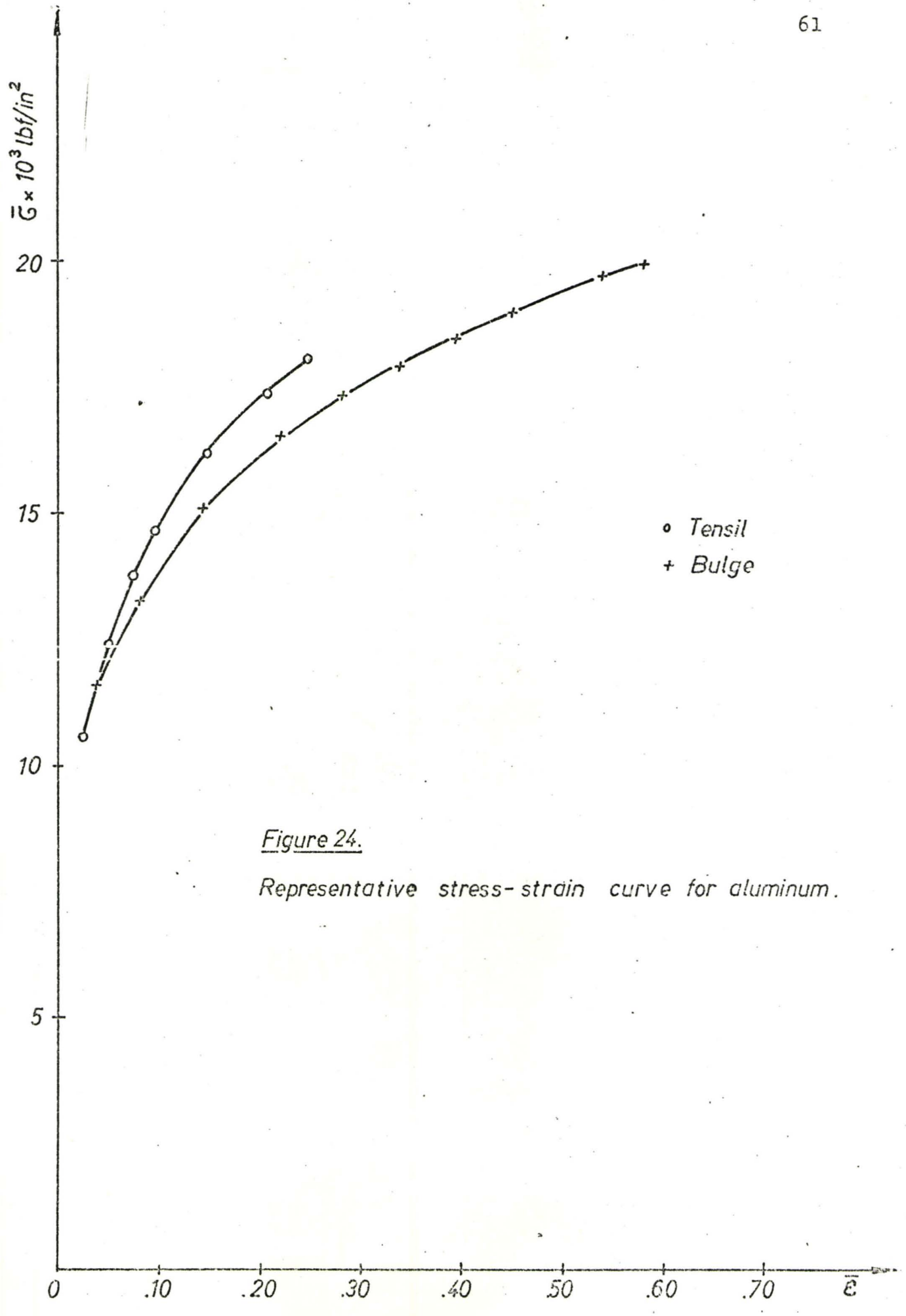

Figure 24.

Representative stress-strain curve for aluminum.

Figure 21 shows clearly that the tensile curve is obtained to a maximum strain of 0.35 while the bulge test gives the curve up to a strain of 0.65 to 0.68.

The advantage of the bulge test over the tensile test is immediately clear on examination of the test curves.

It has to be emphasized that the bulge test also gives a point on a forming limit diagram.

Maximum error in the representative stress - strain curve due to the finite distance over which extension and curvature is measured for low strain is 5% and for strain over 0.25, the error is vanishing.

A photograph of the bulged mild steel specimen is shown in Fig. 23. It can be observed that specimens burst along the rolling direction.

To demonstrate the performance of the equipment on another material, an aluminium alloy sheet .040" thick was tested.

The bulge test and the tensile test results are shown in Fig. 24.

The stress - strain curves are for a specimen aligned in the transverse direction.

The tensile curve is obtained only up to a strain of 0.25 while the bulge curve is up to 0.58.

The difference between the tensile and the bulge test in representative stress magnitudes could be

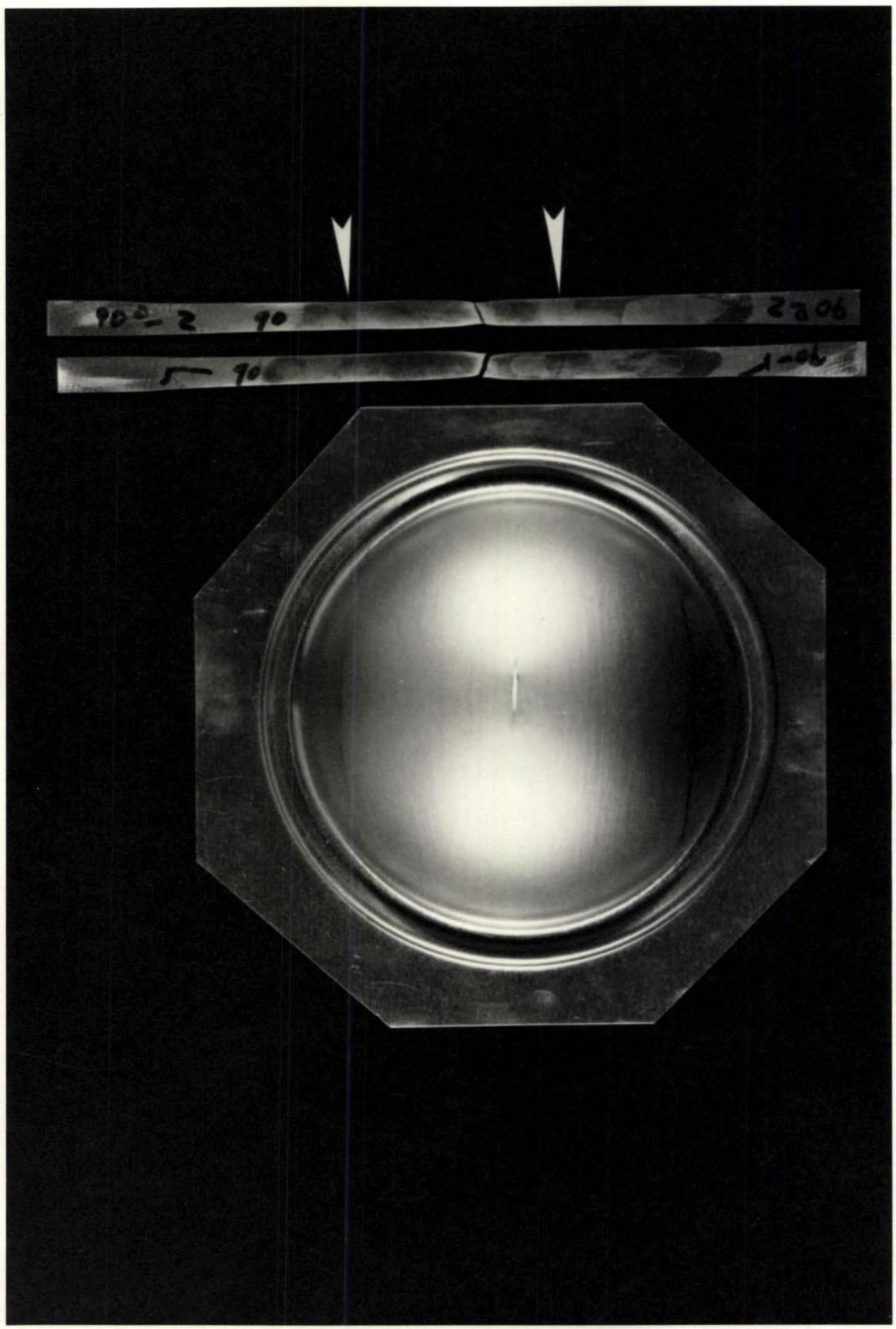

Figure 25. Failure bulge and tensile specimens (aluminum).

explained by normal anisotropy in the sheet.

The average value of R for specimens aligned at 90° with respect to the rolling direction was R = .965.

Figure 25 shows a bulged aluminium specimen placed beside a tensile specimen. A photograph shows very clearly the rolling direction of the sheet and the line of failure along it.

Aluminium has not been fully investigated in all directions with respect to the rolling direction because of limited supply of the material. Therefore further investigation is advised before any general conclusion can be suggested.

7. DISCUSSION

The bulge test has advantages over the tensile test since no special techniques are required to prepare the test-piece. The method used to cut the specimen has no influence on the test as the specimen is clamped at the periphery, while in the tensile test special care must be taken to ensure that the edges of the strip are not work hardened.

The bulge test requires simple equipment since the specimen can be formed using a simple die and a hand pump. The stress - strain curve can be obtained up to higher values of strain than in the tensile test as indicated above. The range of the test covers the range in any real sheet metal forming operation. Even in materials exhibiting very low strain, e.g. as aluminium.

The International Deep Drawing Research Group(29) has investigated the use of the bulge test as a valuable test in a number of countries like Great Britain, Germany, France, Belgium, and Sweden and it was emphasized that the bulge test is a very useful test for research on deep drawing and is very valuable in the determination of forming limit and true stress - strain curve.

At the present moment there is no unification in the bulging die diameter and the standardization of the die is suggested as desirable.

The question of the correlation of the die diameter and the strain was put, and further investigation in this direction is suggested.

At the present moment about 35 units of the extensometer and spherometer designed by Johnson and Duncan (19) are used in Europe and North America.

The primary object of this project was to design and manufacture an improved biaxial test unit. It was hoped that in the course of this project, information and experience would be gained which would materially assist in the development of biaxial test equipment for general research in plasticity and in testing in industrial metal-forming processes.

The bulge test unit designed by the author has certain advantages over the existing unit mainly in the construction of the spherometer and ease of manufacture.

The combined unit of the extensometer and the spherometer is placed in a cylinder with a bottom plate which prevents oil from splashing when the specimen bursts, and makes the testing procedure much cleaner than it used to be.

Total cost of the biaxial test equipment together with the hydraulic system and biaxial test unit including modifications during manufacture, as shown in Fig.26, was $3,400.

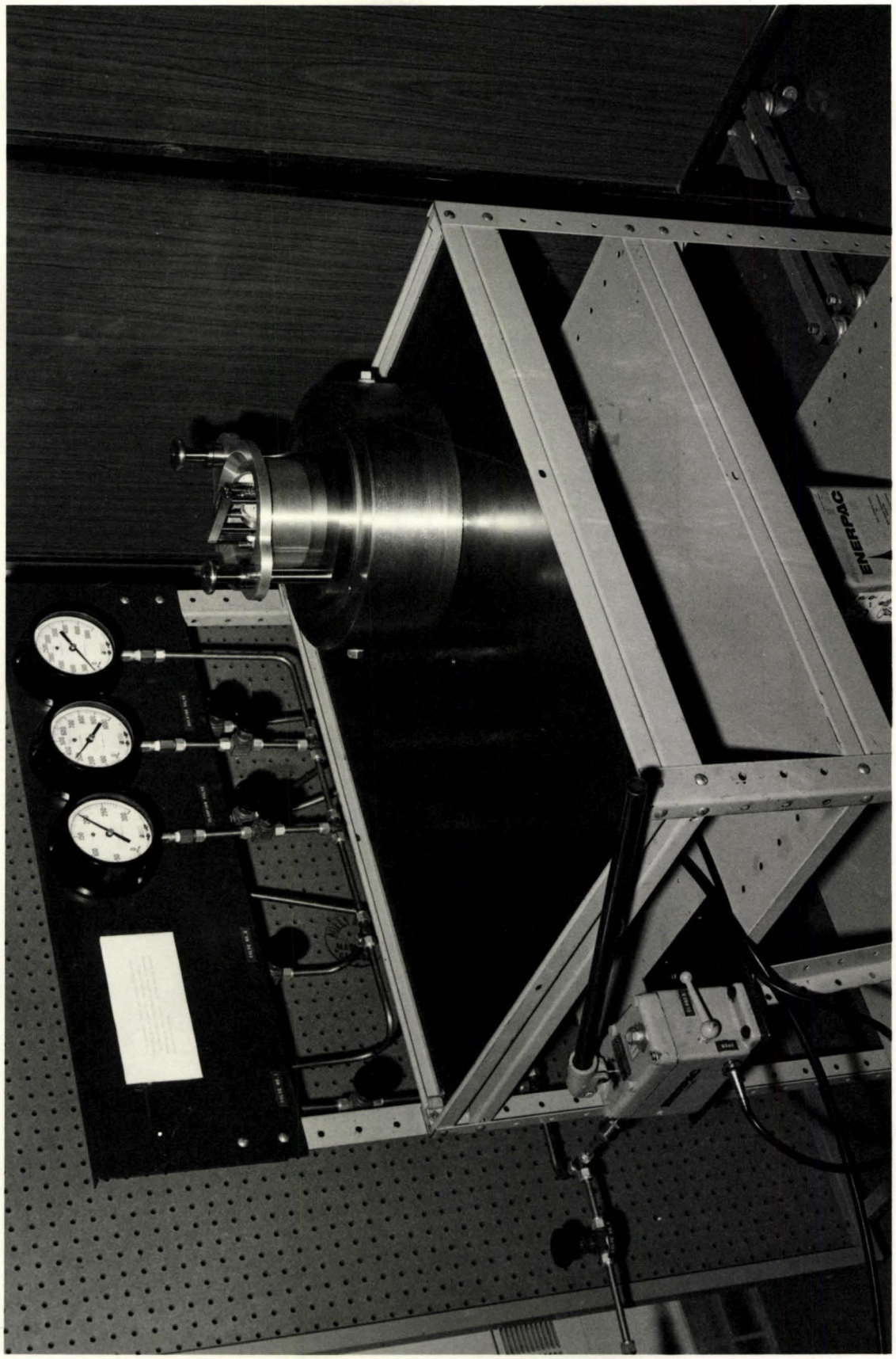

Figure 26. Biaxial test equipment.

If the present design were to be exploited by producing a biaxial test unit commercially in a lot of say 10, the cost should not exceed $2,100.

For a commercially built unit, use of a motor driven pump instead of a hand one should be reconsidered.

It is generally realized that a better understanding of the behaviour of materials in press-shop work must be based on the use of fundamental material properties such as the stress - strain characteristic.

At the present, the stress - strain curve is not used to any great extent for the selection of sheet material for press shop operation.

It is understood that in most sheet-metal working processes (except for deep drawing), average strains involved are not generally as great as the maximum strains in the bulge test; however, the properties of the material are generally only of interest when a sheet fails or is liable to fail in a particular press-shop operation. It is reasonably certain then that knowledge of material properties in these strain ranges will be of great value.

REFERENCES

1. Duncan, J. L., Ph.D. Thesis, University of Manchester, 1968.
2. Bramley, A. N.; Mellor, P. B., Int. J. Mech. Sci., 8, 101, 1966.
3. Chakrabarty, J., Int. J. Mech. Sci., 9, 169, 1970.
4. Duncan, J. L., Int. J. Mech. Sci., 9, 157, 1967.
5. Duncan, J. L., Johnson, Int. J. Mech. Sci., 10, 143, 1968.
6. Duncan, J. L., Johnson, Int. J. Mech. Sci., 10, 157, 1968.
7. Woo, D. M., J. Mech. Engng. Sci., 6, 116, 1969.
8. Venter, R. D., Ph.D. Thesis, McMaster Univ. 1971.
9. Goodwin, Soc. of Automotive Engineers N^{o} 680093, 1968.
10. Marciniak, Z., and Kuczynski, K., Int. J. Mech. Sci., 9, 609, 1967.
11. Sowerby, R., Duncan, J. L., Int. J. Mech. Sci., 13, 217, 1971.
12. Sachs, G., and Lubahn, J. D., ASME Trans., 68, 271, 1946.
13. Brown, W. F., and Sachs, G., ASME Trans., 70, 241, 1948.
14. Hill, R., Phil. Mag. (Ser., 7, 41,) 322, 1133, 1950.
15. Mellor, P. B., J. of Mech. Phys. of Solids, 5, 41, 1956.
16. Bramley, A. N., Mellor, P. B., 5th Machine Tool Design and Research Cont., Birmingham, Sept. 1964.

17. Hill, R., The mathematical theory of plasticity, Oxford 1950.

18. Woo, D. M., Int. J. of Mech. Sci., 6, 303, 1964.

19. Duncan, J. L., Johnson, Sheet Metal Industries, April, 1965.

20. Sachs, G., Espey, G., and Kasik, G. B., ASME Trans., 68, 161, 1946.

21. Lilet, L., Wybo, M., Sheet Metal Ind., 41, 450, 783, 1964.

22. Wilson, I. H., M.Sc. Thesis, University of Manchester, 1968.

23. Sowerby, R., Stability in biaxial straining. (private communication)

24. Bell, R., Duncan, J. L., Wilson, I. H., Proc. Inst. Mech. Engrs., 180 (Pt 3A), 261, 1965.

25. Bell, R., Duncan, J. L., Wilson, I. H., J. Strain Analysis, 2, No. 3, 246, 1967.

26. Duncan, J. L., British Deep Drawing Research Group Colloquim, April 6, 1965.

27. Johnson, W., Duncan, J. L., Kormi, K., Sowerby, R., Travis, F. W., 4th International M.T.D.R. Conference, Advances in Machine Tool Design and Research, Pergamon Press, p. 257, Oxford, 1964.

28. Sowerby, R., Duncan, J. L., Report, Faculty of Engineering ME 171/SM/REP/4.

29. International Deep Drawing Research Group Document No DDR/WGIII/22B/71.

APPENDIX A

Operation Instructions for Bulging Experiment

1. Measure specimen thickness.
2. Shut off valve No. 3 - keep it closed during all operations.
3. Remove the nut from the top of the die.
4. Bleed the hydraulic system:
   (a) Shut off clamping valve.
   (b) Open bulging valve.
   (c) Close hand pump valve and start pumping.
   (d) When air bubbles stop showing up place the specimen into the die, (do not allow any air to remain between the specimen and clamping ring.)
5. Turn down the nut (use pins).
6. Shut off bulging valve and valve No. 2.
7. Open valve No. 1, and clamping valve.

   NOTE: Do not exceed pressure gauge range while increasing pressure in the system.
8. Start pumping until sufficient clamping pressure is reached (700 psi).
9. Shut off clamping valve.
10. Release pressure in the hydraulic system by opening the pump valve.
11. Shut off valve No. 1.
12. Open valve No. 2 and bulging valve.
13. Set up instrument gauges on zero.

14. Place instrument into the locating ring on the die.
15. Close pump valve and start pumping, take reading approximately every .005" indicated on the extensometer gauges.
16. After specimen is bulged release pressure by opening pump valve, open valve No. 1 and No. 2, clamping valve, and the end open the valve of the lowest range pressure gauge.
17. Lift up the instrument and place it back into the carrying box.

APPENDIX B

In the first two columns, the value indicated on the spherometer dial gauge is given and the corresponding radius of curvature.

The sum of the two extensometer gauges is presented in the table as "extensometer reading" and the corresponding strain and thickness ratio can be found.

The thickness variation with the increment of strain for initial thickness .030" is calculated and shown as an example.

SPHEROMETER READING	RADIUS OF CURVATURE	EXTENSOMETER READING	STRAIN	THICKNESS	TO/T RATIO
.001	561.800	.001	.001	.030	1.001
.002	280.901	.002	.007	.030	1.007
.003	187.268	.003	.012	.030	1.012
.004	140.452	.004	.018	.029	1.018
.005	112.363	.005	.023	.029	1.024
.006	93.636	.006	.029	.029	1.029
.007	80.261	.007	.034	.029	1.035
.008	70.229	.008	.040	.029	1.040
.009	62.427	.009	.045	.029	1.046
.010	56.185	.010	.050	.029	1.052
.011	51.078	.011	.056	.028	1.057
.012	46.823	.012	.061	.028	1.063
.013	43.222	.013	.067	.028	1.069
.014	40.136	.014	.072	.028	1.075
.015	37.461	.015	.077	.028	1.080

SPHEROMETER READING	RADIUS OF CURVATURE	EXTENSOMETER READING	STRAIN	THICKNESS	TO/T RATIO
.016	35.120	.016	.083	.028	1.086
.017	33.056	.017	.088	.027	1.092
.018	31.220	.018	.093	.027	1.098
.019	29.578	.019	.099	.027	1.104
.020	28.100	.020	.104	.027	1.109
.021	26.763	.021	.109	.027	1.115
.022	25.547	.022	.114	.027	1.121
.023	24.438	.023	.119	.027	1.127
.024	23.420	.024	.125	.026	1.133
.025	22.485	.025	.130	.026	1.139
.026	21.621	.026	.135	.026	1.145
.027	20.821	.027	.140	.026	1.151
.028	20.078	.028	.145	.026	1.157
.029	19.387	.029	.151	.026	1.162
.030	18.742	.030	.156	.026	1.168

SPHEROMETER READING	RADIUS OF CURVATURE	EXTENSOMETER READING	STRAIN	THICKNESS	TO/T RATIO
.031	18.138	.031	.161	.026	1.174
.032	17.572	.032	.166	.025	1.180
.033	17.041	.033	.171	.025	1.187
.034	16.541	.034	.176	.025	1.193
.035	16.069	.035	.181	.025	1.199
.036	15.624	.036	.186	.025	1.205
.037	15.202	.037	.191	.025	1.211
.038	14.803	.038	.196	.025	1.217
.039	14.425	.039	.201	.025	1.223
.040	14.065	.040	.206	.024	1.229
.041	13.723	.041	.211	.024	1.235
.042	13.397	.042	.216	.024	1.241
.043	13.087	.043	.221	.024	1.248
.044	12.790	.044	.226	.024	1.254
.045	12.507	.045	.231	.024	1.260

SPHEROMETER READING	RADIUS OF CURVATURE	EXTENSOMETER READING	STRAIN	THICKNESS	TO/T RATIO
.046	12.236	.046	.236	.024	1.266
.047	11.977	.047	.241	.024	1.272
.048	11.728	.048	.246	.023	1.279
.049	11.490	.049	.251	.023	1.285
.050	11.261	.050	.256	.023	1.291
.051	11.041	.051	.261	.023	1.298
.052	10.830	.052	.265	.023	1.304
.053	10.626	.053	.270	.023	1.310
.054	10.431	.054	.275	.023	1.317
.055	10.242	.055	.280	.023	1.323
.056	10.060	.056	.285	.023	1.329
.057	9.885	.057	.290	.022	1.336
.058	9.715	.058	.294	.022	1.342
.059	9.552	.059	.299	.022	1.349
.060	9.393	.060	.304	.022	1.355

SPHEROMETER READING	RADIUS OF CURVATURE	EXTENSOMETER READING	STRAIN	THICKNESS	TO/O RATIO
.061	9.240	.061	.309	.022	1.361
.062	9.092	.062	.313	.022	1.368
.063	8.949	.062	.318	.022	1.374
.064	8.810	.064	.323	.022	1.381
.065	8.676	.065	.327	.022	1.387
.066	8.545	.066	.332	.022	1.394
.067	8.419	.067	.337	.021	1.401
.068	8.296	.068	.342	.021	1.407
.069	8.177	.069	.346	.021	1.414
.070	8.061	.070	.351	.021	1.420
.071	7.948	.071	.356	.021	1.427
.072	7.839	.072	.360	.021	1.434
.073	7.732	.073	.365	.021	1.440
.074	7.629	.074	.369	.021	1.447
.075	7.528	.075	.374	.021	1.454

SPHEROMETER READING	RADIUS OF CURVATURE	EXTENSOMETER READING	STRAIN	THICKNESS	TO/T RATIO
.076	7.430	.076	.379	.021	1.460
.077	7.335	.077	.383	.020	1.467
.078	7.242	.078	.388	.020	1.474
.079	7.151	.079	.392	.020	1.480
.080	7.062	.080	.397	.020	1.487
.081	6.976	.081	.401	.020	1.494
.082	6.892	.082	.406	.020	1.501
.083	6.810	.083	.410	.020	1.507
.084	6.730	.084	.415	.020	1.514
.085	6.652	.085	.419	.020	1.521
.086	6.576	.086	.424	.020	1.528
.087	6.501	.087	.428	.020	1.535
.088	6.428	.088	.433	.019	1.542
.089	6.357	.089	.437	.019	1.549
.090	6.287	.090	.442	.019	1.555

SPHEROMETER READING	RADIUS OF CURVATURE	EXTENSOMETER READING	STRAIN	THICKNESS	TO/T RATIO
.091	6.219	.091	.446	.019	1.562
.092	6.153	.092	.451	.019	1.569
.093	6.087	.093	.455	.019	1.576
.094	6.024	.094	.459	.019	1.583
.095	5.961	.095	.464	.019	1.590
.096	5.900	.096	.468	.019	1.597
.097	5.840	.097	.473	.019	1.604
.098	5.782	.098	.477	.019	1.611
.099	5.724	.099	.481	.019	1.618
.100	5.668	.100	.486	.018	1.625
.101	5.613	.101	.490	.018	1.632
.102	5.559	.102	.494	.018	1.639
.103	5.506	.103	.499	.018	1.647
.104	5.454	.104	.503	.018	1.654
.105	5.403	.105	.507	.018	1.661

SPHEROMETER READING	RADIUS OF CURVATURE	EXTENSOMETER READING	STRAIN	THICKNESS	TO/O RATIO
.106	5.353	.106	.512	.018	1.668
.107	5.304	.107	.516	.018	1.675
.108	5.256	.108	.520	.018	1.682
.109	5.209	.109	.524	.018	1.689
.110	5.162	.110	.529	.018	1.697
.111	5.117	.111	.533	.018	1.704
.112	5.072	.112	.537	.018	1.711
.113	5.028	.113	.541	.017	1.718
.114	4.985	.114	.546	.017	1.726
.115	4.943	.115	.550	.017	1.733
.116	4.901	.116	.554	.017	1.740
.117	4.860	.117	.558	.017	1.748
.118	4.820	.118	.562	.017	1.755
.119	4.781	.119	.567	.017	1.762
.120	4.742	.120	.571	.0.7	1.770

SPHEROMETER READING	RADIUS OF CURVATURE	EXTENSOMETER READING	STRAIN	THICKNESS	TO/T RATIO
.121	4.703	.121	.575	.017	1.777
.122	4.666	.122	.579	.017	1.784
.123	4.629	.123	.583	.017	1.792
.124	4.593	.124	.587	.017	1.799
.125	4.557	.125	.591	.017	1.807
.126	4.522	.126	.596	.017	1.814
.127	4.487	.127	.600	.016	1.822
.128	4.453	.128	.604	.016	1.829
.129	4.420	.129	.608	.016	1.837
.130	4.387	.130	.612	.016	1.844
.131	4.354	.131	.616	.016	1.852
.132	4.322	.132	.620	.016	1.859
.133	4.291	.133	.624	.016	1.867
.134	4.260	.134	.628	.016	1.874
.135	4.229	.135	.632	.016	1.882

SPHEROMETER READING	RADIUS OF CURVATURE	EXTENSOMETER READING	STRAIN	THICKNESS	TO/T RATIO
.136	4.199	.136	.636	.016	1.889
.137	4.169	.137	.640	.016	1.897
.138	4.140	.138	.644	.016	1.905
.139	4.111	.139	.648	.016	1.912
.140	4.083	.140	.652	.016	1.920
.141	4.055	.141	.656	.016	1.928
.142	4.027	.142	.660	.016	1.935
.143	4.000	.143	.664	.015	1.943
.144	3.973	.144	.668	.015	1.951
.145	3.947	.145	.672	.015	1.959
.146	3.921	.146	.676	.015	1.966
.147	3.895	.147	.680	.015	1.974
.148	3.870	.148	.684	.015	1.982
.149	3.845	.149	.688	.015	1.990
.150	3.820	.150	.692	.015	1.998

SPHEROMETER READING	RADIUS OF CURVATURE	EXTENSOMETER READING	STRAIN	THICKNESS	TO/T RATIO
.151	3.796	.151	.696	.015	2.005
.152	3.772	.152	.700	.015	2.013
.153	3.748	.153	.704	.015	2.021
.154	3.725	.154	.708	.015	2.029
.155	3.702	.155	.711	.015	2.037
.156	3.679	.156	.715	.015	2.045
.157	3.657	.157	.719	.015	2.053
.158	3.635	.158	.723	.015	2.061
.159	3.613	.159	.727	.015	2.069
.160	3.591	.160	.731	.014	2.077
.161	3.570	.161	.735	.014	2.085
.162	3.549	.162	.738	.014	2.093
.163	3.528	.163	.742	.014	2.101
.164	3.508	.164	.746	.014	2.109
.165	3.487	.165	.750	.014	2.117
.166	3.467	.166	.754	.014	2.125

SPHEROMETER READING	RADIUS OF CURVATURE	EXTENSOMETER READING	STRAIN	THICKNESS	TO/T RATIO
.167	3.448	.167	.757	.014	2.133
.168	3.428	.168	.761	.014	2.141
.169	3.409	.169	.765	.014	2.149
.170	3.390	.170	.769	.014	2.157
.171	3.371	.171	.773	.014	2.165
.172	3.352	.172	.776	.014	2.174
.173	3.334	.173	.780	.014	2.182
.174	3.416	.174	.784	.014	2.190
.175	3.298	.175	.788	.014	2.198
.176	3.280	.176	.791	.014	2.206
.177	3.263	.177	.795	.014	2.215
.178	3.245	.178	.799	.013	2.223
.179	3.228	.179	.803	.013	2.231
.180	3.211	.180	.806	.013	2.239
.181	3.194	.181	.810	.013	2.248
.182	3.178	.182	.814	.013	2.256

APPENDIX C

Biaxial Test Unit Calibration

The extensometer and the spherometer gauges are set up to zero by placing the unit on a surface plate.

The extensometer is removed from the unit and reset to zero. In order to get the correct setting, plasticine is used so that the probes are kept apart at the constant distance. Distance that is marked on a soft aluminum plate, and measured with a microscope.

The above described setting was repeated a number of times with increment .005" indicated on each dial gauge.

The least square method was used for fitting a curve into the obtained data points, and finally characteristic curve for the extensometer was established:

$$Y = (X - .36023110)/.30184298$$

The spherometer has not required calibration as such but rather checking the value given by the dial gauge reading with the value given by a micrometer.

APPENDIX D

Stress - Strain Curve Calculation

The program for stress - strain calculation and curve plottings is shown.

The readings of the extensometer ($a_1 + a_2$), bulging pressure and spherometer are shown and calculated values of strain, stress and radius of curvature are presented.

VALUE A1+A2 /IN/

.004 .017 .027 .039 .054 .070 .079 .091
.105 .120 .139

PRESSURE /PSI/

210.000 450.000 570.000 670.000 740.000 800.000 810.000 830.000
840.000 840.000 840.000

SPHEROMETER READINGS /IN/

.047 .085 .104 .121 .137 .151 .157 .166
.174 .182 .191

A1+A2	E	TO/T	T	R	SIGMA
4	.022	1.022	.029	11.977	42854.512
17	.092	1.097	.027	6.652	54709.194
27	.145	1.156	.026	5.454	59870.194
39	.206	1.228	.024	4.703	64510.251
54	.279	1.322	.023	4.169	67992.234
70	.355	1.426	.021	3.796	72195.403
79	.397	1.487	.020	3.657	73394.574
91	.450	1.569	.019	3.467	75259.024
105	.512	1.668	.018	3.316	77425.319
120	.575	1.777	.017	3.178	79066.871
139	.653	1.921	.016	3.037	81657.079

XMIN= 2.208557E-02 XMAX= 6.526467E-01. YMIN= 4.285451E+04 YMAX= 8.165708E+04. 11 POINTS PLOTTED.

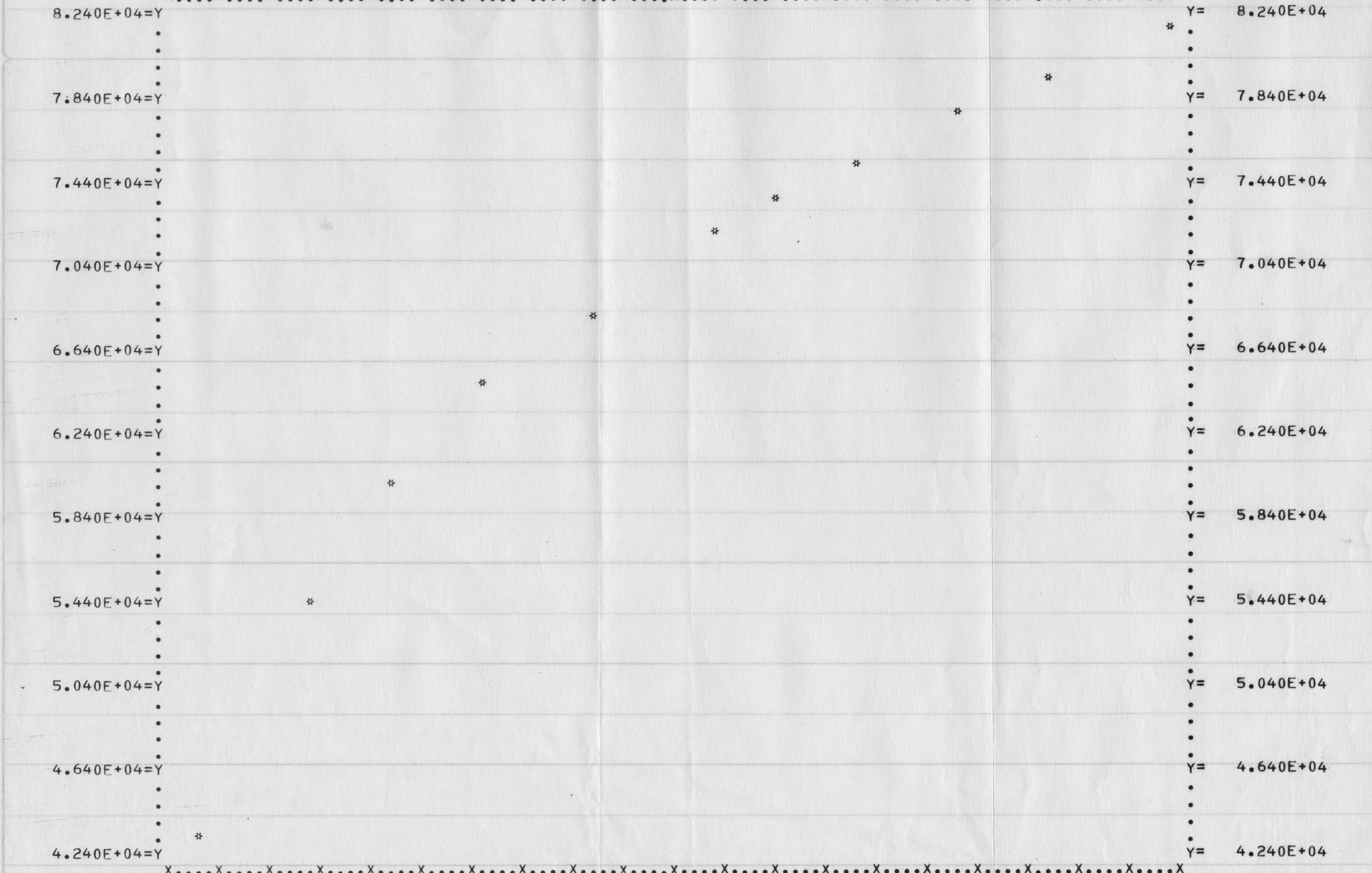

```
HVEA.                                                    ALBERTIN P
RUN(S)
SETINDF.
REDUCF.
LGO.
'          6400 END OF RECORD
      PROGRAM TST (INPUT,OUTPUT,TAPE5=INPUT,TAPE6=OUTPUT)
      DIMENSION Z(24),P(24),C(24),A(24),B(24)
      N=24
      NN=11
      READ(5,55) (Z(I),I=1,N)
      READ(5,55) (P(I),I=1,N)
      READ(5,55) (C(I),I=1,N)
 55   FORMAT(8F10.3)
      WRITE(6,50)
 50   FORMAT(1H1,5X,*VALUE A1+A2 /IN/*,/)
      WRITE(6,56) (Z(I),I=1,NN)
      WRITE(6,51)
 51   FORMAT(/,5X,*PRESSURE PSI*,/)
      WRITE(6,56) (P(I),I=1,NN)
      WRITE(6,52)
 52   FORMAT(/,5X,*SPHEROMETER READINGS /IN/*,/)
      WRITE(6,56) (C(I),I=1,NN)
 56   FORMAT(8F10.3)
      WRITE(6,20)
 20   FORMAT(//,18X,*A1+A2*,15X,*E*,14X,*T0/T*,16X,*T*,13X,*R*,12X,*SIGM
     1A*,///)
      A0=-.36023110
      A1=0.30184298
      D0=-A0/A1
      DO 10 I=1,NN
      W=Z(I)
      U=(W-A0)/A1
      D1=U
```

```
      DP=D1/D0
      E=2.*ALOG(DP)
      RU=U-D0
      TOT=(1.+RU/D0)**2
      THIC=0.030
      T=THIC/TOT
      R=(1.060*1.060+C(I)*C(I))/(2.*C(I))
      SIGMA=(P(I)*R)/(2.*T)
      F=W*1000.
      WRITE(6,21)F,E,TOT,T,R,SIGMA
   21 FORMAT(12X,F10.0,3X,F16.3,1X,F16.3,1X,F16.3,1X,F14.3,1X,F16.3,/)
      A(I)=E
      B(I)=SIGMA
      X=A(I)
      Y=B(I)
      CALL PLOTPT(X,Y,4)
   10 CONTINUE
      CALL OUTPLT
      STOP
      END
'       END OF RECORD
.004      .017      .027      .039      .054      .070      .079      .09
.105      .120      .139

210.      450.      570.      670.      740.      800.      810.      830.
840.      840.      840.

.047      .085      .104      .121      .137      .151      .157      .166
.174      .182      .191

'          END OF FILE
```